University Library

MINERVA ACCESS

A gateway to Melbourne's research publications

Minerva Access is the Institutional Repository of The University of Melbourne

Author/s:
Lopez-Bravo, C;Vincent, CL;Huang, Y;Lane, TP

Title:
Impacts of the Madden-Julian Oscillation on Widespread Heavy Rainfall Over the Western Region of the Maritime Continent: Sumatra

Date:
2025-10-16

Citation:
Lopez-Bravo, C., Vincent, C. L., Huang, Y. & Lane, T. P. (2025). Impacts of the Madden-Julian Oscillation on Widespread Heavy Rainfall Over the Western Region of the Maritime Continent: Sumatra. Journal of Geophysical Research Atmospheres, 130 (19), https://doi.org/10.1029/2025JD043493.

Persistent Link:
https://hdl.handle.net/11343/362589

License:
CC BY-NC

Check for updates

JGR Atmospheres

RESEARCH ARTICLE
10.1029/2025JD043493

Impacts of the Madden-Julian Oscillation on Widespread Heavy Rainfall Over the Western Region of the Maritime Continent: Sumatra

Clemente Lopez-Bravo[1,2], Claire L. Vincent[2,3,4], Yi Huang[2,3,4], and Todd P. Lane[2,3,4]

[1]Climate Change Research Centre, The University of New South Wales, Sydney, NSW, Australia, [2]ARC Centre of Excellence for Climate Extremes, Sydney, NSW, Australia, [3]School of Geography, Earth and Atmospheric Sciences, The University of Melbourne, Melbourne, VIC, Australia, [4]ARC Centre of Excellence for 21st Century Weather, Melbourne, VIC, Australia

Abstract The Precipitation Severity Index (PSI) is used to examine the occurrence of and mechanisms behind widespread persistent rainfall events in Sumatra. Analysis of cloud properties from Himawari-8 is combined with data from IMERG and ERA5 to explore new results about changes in cloud properties relating to heavy rainfall and intraseasonal variability. This study brings a fresh angle to the challenge of understanding the Madden-Julian Oscillation (MJO) modulation of cloud and precipitation over Sumatra by examining changes in the total cloud area and, more importantly, changes in the cold cloud tops that indicate the deepest convection. Although widespread cold clouds are likely regardless of MJO phase, the enhanced prevalence of cold tops requires the support of the large-scale convective envelope. These results provide insight about how the MJO influences the nature as well as the amount of convection. Heavy rainfall is shown to make a larger percentage contribution to the total rainfall during the MJO-enhanced convection phases (2-3-4) over Sumatra. This contribution is suggested to be related to a higher prevalence of cold cloud core areas in phases 2 and 4. In phase 3, there is a remarkable increase in the percentage contribution of heavy rainfall in the cold cloud area but a relatively lower prevalence of the coldest cloud core area, suggesting large-scale environmental support for heavy rainfall but not necessarily the most intense convection. These results exemplify the role of mesoscale processes and cloud microphysics in modulating the MJO-scale modulation of rainfall.

Plain Language Summary Heavy rainfall is a hazard in the Maritime Continent (MC). However, the amount of rain that may be considered a heavy or extreme event varies between definitions. The heavy rainfall and cloud characteristics are investigated using a local approach and island-scale dimension in Sumatra. This work uses satellite-derived rainfall and cloud products from IMERG and Himawari-8, respectively, to explore the variation and frequency of heavy tropical rainfall during December, January, and February in the western region of the MC. This investigation also identifies frequent island-scale heavy rainfall in central Sumatra between 2001 and 2021 influencing the rainfall amount over Singapore and the Malay Peninsula, and the results also show evidence of the effects of the Madden-Julian Oscillation (MJO) on the rainfall variations over the region. Another important finding shows that the significant inland contribution of seasonal rainfall occurs mainly in the active phases of the MJO (phase 3). Additionally, the analysis of cloud structures reveals widespread cloud presence in heavy rainfall events regardless of the MJO phase. This work also presents evidence of the relationship between widespread heavy rainfall, intraseasonal and diurnal variability, and cloud properties from a mesoscale perspective.

Key Points:

- How intraseasonal variability contributes to heavy island-scale rainfall over Sumatra during the austral summer
- Satellite data are used to study the links between heavy rainfall and the diurnal evolution of mesoscale convective systems in Sumatra
- Cloud and cold core areas vary with the MJO phase, indicating that the MJO modifies the characteristics of the convective tower and the MCSs

Supporting Information:

Supporting Information may be found in the online version of this article.

Correspondence to:

C. Lopez-Bravo,
c.lopez_bravo@unsw.edu.au

Citation:

Lopez-Bravo, C., Vincent, C. L., Huang, Y., & Lane, T. P. (2025). Impacts of the Madden-Julian Oscillation on widespread heavy rainfall over the western region of the Maritime Continent: Sumatra. *Journal of Geophysical Research: Atmospheres*, *130*, e2025JD043493. https://doi.org/10.1029/2025JD043493

Received 24 JAN 2025
Accepted 18 SEP 2025

Author Contributions:

Conceptualization: Clemente Lopez-Bravo, Claire L. Vincent, Yi Huang, Todd P. Lane
Data curation: Clemente Lopez-Bravo
Formal analysis: Clemente Lopez-Bravo
Funding acquisition: Claire L. Vincent, Todd P. Lane
Investigation: Clemente Lopez-Bravo
Methodology: Clemente Lopez-Bravo, Claire L. Vincent, Yi Huang, Todd P. Lane
Software: Clemente Lopez-Bravo
Supervision: Claire L. Vincent, Yi Huang, Todd P. Lane
Writing – original draft: Clemente Lopez-Bravo

© 2025 The Author(s).
This is an open access article under the terms of the Creative Commons Attribution-NonCommercial License, which permits use, distribution and reproduction in any medium, provided the original work is properly cited and is not used for commercial purposes.

1. Introduction

The Maritime Continent (MC) experiences some of the most intense deep convection on Earth (Ruppert & Chen, 2020; Zipser et al., 2006). The deep convection across the Indo-Pacific warm pool shows scale interactions from diurnal to intraseasonal scales (Birch et al., 2016). Rainfall and cloud populations have well-defined patterns on monthly and seasonal scales where the maximum amount of rainfall generally occurs over the mountains and coastal areas (Lopez-Bravo et al., 2023b; Mori et al., 2004; Peatman et al., 2014, 2021; Vincent & Huang, 2022; Vincent & Lane, 2016). However, daily and subdaily variations in the intensity and frequency of rainfall are driven by different mechanisms that may affect the predictability of the convective systems and heavy rainfall over Sumatra.

Writing – review & editing:
Clemente Lopez-Bravo, Claire L. Vincent, Yi Huang

Studies of rainfall processes show the importance of mesoscale convective systems (MCSs) as the main source of precipitation in the tropics and have also presented evidence on the links between MCSs and heavy rainfall (Crook et al., 2024; Roca & Fiolleau, 2020; Schumacher & Rasmussen, 2020). Schumacher and Rasmussen (2020) showed that the contribution of extreme rainfall to total rainfall depends on many factors linked to the convective environment of MCSs, including convective organization, internal dynamics, and thermodynamical and microphysical processes. Zipser et al. (2006), Nesbitt et al. (2006), and Roca and Fiolleau (2020) emphasized the importance of the lifetime of organized convection and morphological aspects to explain the extreme precipitating storms over land and tropical oceans.

Although MCSs and diurnally forced convection are two of the major contributors to heavy rainfall over land and ocean in the tropics, heavy rainfall is strongly modulated by large-scale tropical variability particularly the Madden-Julian Oscillation (MJO), the dominant mode of intraseasonal variability of rainfall, along with equatorially trapped waves (Baranowski et al., 2016, 2020; Da Silva & Matthews, 2021; Peatman et al., 2023; Vincent & Lane, 2016; Xavier et al., 2014). The MJO consists of eastward-propagating convective and circulation anomalies with a 30–60-day period, shaping rainfall, cloud populations, and atmospheric circulation across the Indo-Pacific warm pool (Madden & Julian, 1971).

Several studies have specifically examined how MCSs themselves are modulated by these larger-scale modes of equatorial rainfall variability in the MC B. Mapes et al. (2006), Kiladis et al. (2009), Dias et al. (2017), Cheng et al. (2023), and Crook et al. (2024), and more generally, others have tested hypotheses about rainfall variations over the major islands of the MC and the effects of intraseasonally induced extreme rainfall over Sumatra (Baranowski et al., 2020; Birch et al., 2016; Ferrett et al., 2020; Lopez-Bravo et al., 2023a, 2023b; Peatman et al., 2014, 2021; Rauniyar & Walsh, 2011; Short et al., 2019; Vincent & Lane, 2016). Birch et al. (2016) and Wei et al. (2020) proposed that the large-scale convective environment can modify the land-sea-breeze circulation and rainfall patterns by equatorial wave dynamics and radiative processes, for example, the enhanced convective phase of the MJO. The modulation of the diurnal cycle and interplay with Convectively coupled Kelvin waves (CCKWs) were also studied by Baranowski et al. (2016) and Senior et al. (2023). In parallel, Vincent and Lane (2016), Short et al. (2019), and Natoli and Maloney (2023a); Natoli and Maloney (2023b) suggest variations of background wind flow from the MJO passage over the MC are also essential in driving the land-sea-breeze circulations and convection.

There have been numerous studies focusing on the composite rainfall patterns under various modes of variability (Peatman et al., 2014, 2021, 2023; Senior et al., 2023; Vincent & Lane, 2017) and detailed studies of diurnally propagating squall lines in the MC (Chan et al., 2019; Lopez-Bravo et al., 2023a; Peatman et al., 2023). However, relatively few studies have examined the processes, thermodynamical support, and cloud populations associated with widespread island-scale rainfall events (Vincent & Lane, 2017; Da Silva & Matthews, 2021). These events are of considerable interest because, although originating from populations of individual convective cells, the resulting rainfall can be associated with widespread rainfall extending over the island, which we refer to as island-scale rainfall. This indicates a strong up-scale link between large-scale forcing, convective-scale processes, and rainfall over land. Heavy rainfall events are also noteworthy due to their associated hydrological hazards. Although not a focus of this paper, it is evident that rainfall impacting multiple locations on a single day can lead to pressure on emergency management services and flooding across whole river basin areas.

This study examines island-scale heavy rainfall events in Sumatra specifically addressing the following science questions:

1. What is the contribution of widespread, persistent heavy rainfall to the total rainfall climate in Sumatra?
2. How do changes in the large-scale convective environment associated with the MJO map onto changes in widespread, persistent heavy rainfall in Sumatra?
3. How does the morphology of the cloud population during widespread, persistent heavy rainfall events in Sumatra vary with the MJO in particular with reference to the cold cloud area and the cold cloud core area?

Our study provides a detailed analysis of heavy island-scale rainfall and the effects of intraseasonal-scale variability on rainfall patterns and cold cloud tops associated with heavy rainfall events over Sumatra during the austral summer. We define a heavy rainfall event by analyzing the intensity, persistence, and spatial distribution of rainfall over land in Sumatra using the Precipitation Severity Index (Caldas-Alvarez et al., 2022; Piper et al., 2016) and Integrated Multi-satellite Retrievals for Global Precipitation Measurement (IMERG), version 6,

21698996, 2025, 19, Downloaded from https://agupubs.onlinelibrary.wiley.com/doi/10.1029/2025JD043493 by National Health And Medical Research Council, Wiley Online Library on [27/11/2025]. See the Terms and Conditions (https://onlinelibrary.wiley.com/terms-and-conditions) on Wiley Online Library for rules of use; OA articles are governed by the applicable Creative Commons License

21698996, 2025, 19, Downloaded from https://agupubs.onlinelibrary.wiley.com/doi/10.1029/2025JD043493 by National Health And Medical Research Council, Wiley Online Library on [27/11/2025]. See the Terms and Conditions (https://onlinelibrary.wiley.com/terms-and-conditions) on Wiley Online Library for rules of use; OA articles are governed by the applicable Creative Commons License

for the period 2001–2021. Cold cloud tops were identified employing geostationary measurements from Himawari-8 for austral summer, 2016–2021 (Lopez-Bravo et al., 2021a, 2021b), and reanalysis data from the European Center for Medium-Range Weather Forecasts (ECMWF) 5th Generation Reanalysis (ERA5, Hersbach et al., 2020), covering 2001–2021.

Section 2 presents the data sets and methods used in the current study. Then, Section 3 examines a composite analysis of heavy rainfall events, clustering analysis of diurnal signatures, the fraction of heavy rainfall to seasonal rainfall by MJO phases, and moisture flux convergence for austral summer, December-January-February (DJF). Next, we present the cold cloud area and cold cloud core diurnal distributions over Sumatra for six austral summers. Finally, the discussion and conclusions are found in Sections 4 and 5.

2. Data and Methods

2.1. IMERG Data Collection

IMERG version 6 (G. Huffman, Bolvin, et al., 2019; G. Huffman, Stocker, et al., 2019; G. J. Huffman et al., 2020), at 0.1° and 30-min resolution, is utilized to analyze the heavy rainfall patterns over Sumatra. This study uses hourly accumulated precipitation and daily accumulated rainfall during the austral summer DJF from 2001 to 2021 to estimate the heavy rainfall in Sumatra. Tan et al. (2019) and Da Silva and Matthews (2021) showed that IMERG can capture the diurnal cycle (DC) of rainfall over the Maritime Continent well. Ramadhan et al. (2022) further evaluated IMERG using ground-based rain gauge data and found that it performs well in detecting heavy rainfall with a Kling-Gupta Efficiency (KGE) > 0.4 in many locations. However, they also reported that IMERG tends to overestimate light rainfall and has lower accuracy during extended wet periods. The DC of precipitation based on IMERG is consistent with previous studies in which ground observations and active retrievals were used (Crook et al., 2024; Da Silva et al., 2021; Lopez-Bravo et al., 2023b; Mori et al., 2004; Qian, 2008).

2.2. The Satellite-Derived Data Set From Himawari-8

Satellite-based cloud products derived from Himawari-8 Advanced Himawari Imager (AHI) were utilized to explore the cold cloud tops related to MCSs during heavy rainfall events in Sumatra. Himawari-8 AHI has band-dependent spatial resolutions (JMA, 2017): 0.5 km (Band 3, visible), 1.0 km (Bands 1, 2, 4, visible/near-IR), and 2.0 km (Bands 5–16, infrared) with a 10-min full-disk cadence. Two satellite-derived data sets cover the MC and Australian region at the same Himawari-8 AHI spatial resolution and hourly temporal resolution for DJF from 2016 to 2021: Level-1 includes the brightness temperature of 16 spectral bands of Himawari-8 AHI (Lopez-Bravo et al., 2021a) and Level-2 products provide derived satellite cloud properties, for example, cloud top temperature, cloud top height, cloud optical depth, and a classification of cloud type based on the cloud top (Lopez-Bravo et al., 2021b).

2.3. Cold Cloud Area and Cold Cloud Core Identification

Fiolleau and Roca (2013), Feng et al. (2018, 2021), Schumacher and Rasmussen (2020), and Lopez-Bravo et al. (2023b) have used the brightness temperature from geostationary satellite data for automated cloud object detection to identify cold cloud tops regionally or globally. In this study, cold cloud tops were identified via a multilevel thresholding technique for satellite image segmentation as follows:

1. Gaussian filtering with a standard deviation from 1.5 to 2.5 is used to reduce the noise present in each scene of brightness temperature at the 10.4 μm ($BT_{10.4}$) spectral band from Himawari-8 AHI.
2. Feature detection based on a multilevel thresholding technique was used to identify cold cloud areas and cold cloud cores based on $BT_{10.4}$. For cold cloud areas, a threshold of 253 K was used to discriminate between clear sky and cloud systems, whereas 240 K was applied to delineate the cold cloud area. For cold cloud cores, thresholds of 220, 217, and 213 K were used to improve detection sensitivity across a range of cloud intensities. Among these, the minimum thresholds of 240 K (cold cloud areas) and 213 K (cold cloud cores) were adopted to define the final target regions. This multilevel thresholding approach enhances the detection of cloud structures with varying intensity, following the methodologies of B. E. Mapes and Houze (1993), Fiolleau and Roca (2013), Machado et al. (1993), Vila et al. (2008), Feng et al. (2018), and Lopez-Bravo et al. (2023a, 2023b).

3. Image segmentation was used to extract and label every single cold cloud area and cold cloud core derived from the previous step based on the watershed algorithm following Beucher (1979) and Heikenfeld et al. (2019).

Cold areas were identified at each timestamp and subsequently linked to the maximum rainfall regions to extract features during the active precipitation event.

2.4. Heavy Rainfall Events-Precipitation Severity Index

The island-scale heavy rainfall events over Sumatra were identified by the Precipitation Severity Index (PSI) and satellite-based rainfall estimates from IMERG for DJF, 2001–2021. The PSI was initially derived from the Storm Severity Index (Leckebusch et al., 2008; Pinto et al., 2012). In this study, we calculate the PSI on the native IMERG grid following the methodology of Piper et al. (2016), Pinto et al. (2012), and Caldas-Alvarez et al. (2022). The detection of heavy rainfall events is based on the PSI that includes rainfall intensity of each grid point over Sumatra, time persistence of 2 days, and rainfall area (spatial coverage). To illustrate the spatial extent and intensity of rainfall, four heavy rainfall events are shown in Figure S1 in Supporting Information S1. The PSI therefore detects widespread, long-lived heavy rainfall and is less sensitive to short-duration or isolated rainfall with small spatial coverage. A heavy rainfall event was assigned when PSI values exceeded the 80th percentile PSI for the 20-year DJF period detecting 371 events. To verify the consistency of the result, the PSI was calculated using the 80th, 90th, and 95th percentiles of accumulated daily rainfall for the analyzed period (not shown). For description of the PSI see Appendix A.

2.5. Heavy Rainfall Events-MJO Index, PSI, and Percentage Contribution

The evolution and strength of the MJO are commonly represented by the Real-time Multivariate MJO (RMM) index (Wheeler & Hendon, 2004). The RMM index is based on the first two empirical orthogonal functions of a multivariate field composed of zonal wind in the lower (850 hPa) and the upper troposphere (200 hPa) and the outgoing longwave radiation (OLR) at the top of the atmosphere. This study uses the PSI and the RMM index as the basis for the composites of cold cloud tops and rainfall. The dates classified as heavy rainfall events were subcategorised by MJO phase and amplitude. (a) PSI was used to identify heavy rain events during DJF between 2001 and 2021. (b) Each day of the heavy rainfall event was assigned to one of the eight MJO phases based on the RMM index with an amplitude greater than or equal to 0.8. (c) Composite precipitation analyses were calculated for each MJO phase and for phases 7-8-1 (which we refer to as the suppressed convective phases of the MJO over the western MC) and 2-3-4 (the enhanced convective phases of the MJO over the western MC). The list of heavy rain days was also used to analyze satellite-derived cloud top features derived from Himawari-8 AHI during six austral summers between 2016 and 2021.

The percentage contribution to the total rainfall during the MJO phase was calculated based on the composite of daily rainfall on days when heavy rainfall events were identified over land in Sumatra based on the RMM index and PSI. Although identifying heavy rainfall events is restricted to land areas, the composite includes rainfall values over the surrounding ocean and nearby countries to capture the broader spatial context of these events. This approach allows us to examine the regional structure and extent of the associated convective systems and large-scale rainfall patterns, which often extend beyond the island.

2.6. Heavy Rainfall Clustering Over Land Sumatra

Classifying and identifying diurnal patterns of a heavy rainfall event are relevant to understanding the mechanism of severe weather in Sumatra. Therefore, the diurnally accumulated rainfall time series on heavy rainfall days are clustered into six classes for heavy rainfall events over land Sumatra for austral summer. It is important to note here that we consider the aggregate rainfall over Sumatra. Different processes are included in this aggregation, including coastal and inland topographically forced convection. We do not aim to separate these processes but to understand the large-scale diurnal aspects of heavy rainfall days. A hierarchical clustering algorithm (Hastie et al., 2009) is employed on the heavy rainfall events from the PSI. Each sample starts as a cluster (agglomerative), and after that, two clusters are merged according to a linkage criterion (e.g., weighted average linkage clustering). This process of merging is repeated until all samples converge in the same cluster and create a hierarchical tree-like structure named a dendrogram by considering the intracluster variance to select the optimal

21698996, 2025, 19, Downloaded from https://agupubs.onlinelibrary.wiley.com/doi/10.1029/2025JD043493 by National Health And Medical Research Council, Wiley Online Library on [27/11/2025]. See the Terms and Conditions (https://onlinelibrary.wiley.com/terms-and-conditions) on Wiley Online Library for rules of use; OA articles are governed by the applicable Creative Commons License

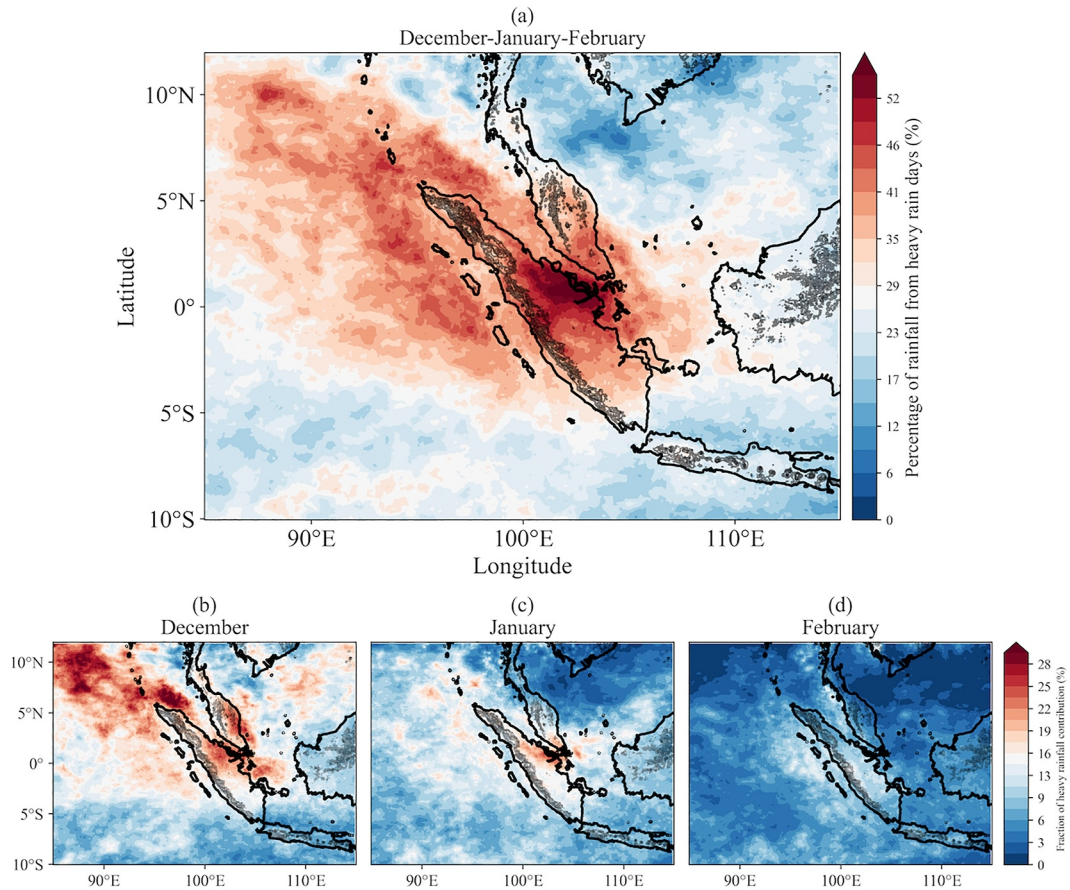


Figure 1. Composite of the percentage of rainfall from heavy rainfall events in Sumatra to accumulated seasonal precipitation for austral summer (2001–2021) from IMERG data. (a) December-January-February. Fraction of the seasonal heavy rainfall contribution by month: (b) December, (c) January, and (d) February. These fractions are not meant to represent monthly heavy rainfall contributions relative to monthly total rainfall as in panel (a). Instead, these panels show how the seasonal heavy rainfall contribution is distributed across the individual months expressed as a fraction of total heavy rainfall contribution. Please note that the color scale has been adjusted for better representation. The gray contour lines indicate topography.

number of clusters and grouping samples to create a branch of the dendrogram (Fiddes et al., 2021; Hastie et al., 2009).

2.7. Reanalysis Data ERA5

The European Center for Medium-Range Weather Forecasts (ECMWF) Reanalysis 5th Generation (ERA5) data are used to compute composite analyses of zonal and meridional wind components. First, wind components were vertically averaged over 925–850 hPa for austral summer from 2016 to 2021 by MJO phases. Similar composite analysis was performed for the vertically integrated moisture flux convergence from the surface of the Earth to the top of the atmosphere and for streamlines to verify the effects of the enhanced and suppressed convective phases of the MJO over the large-scale patterns and moisture availability. The MJO phases were selected by the RMM index, filtering the dates when the amplitude of the RMM index was greater than or equal to 0.8 to include significant MJO events.

3. Results

3.1. Austral Summer Island-Scale Heavy Rainfall

The percentage of rainfall from heavy rainfall events for austral summer (DJF: 2001–2021) is shown in Figure 1a. Central Sumatra exhibits the maximum percentage of heavy rainfall contribution at 55% and this decreases in the

21698996, 2025, 19, Downloaded from https://agupubs.onlinelibrary.wiley.com/doi/10.1029/2025JD043493 by National Health And Medical Research Council, Wiley Online Library on [27/11/2025]. See the Terms and Conditions (https://onlinelibrary.wiley.com/terms-and-conditions) on Wiley Online Library for rules of use; OA articles are governed by the applicable Creative Commons License

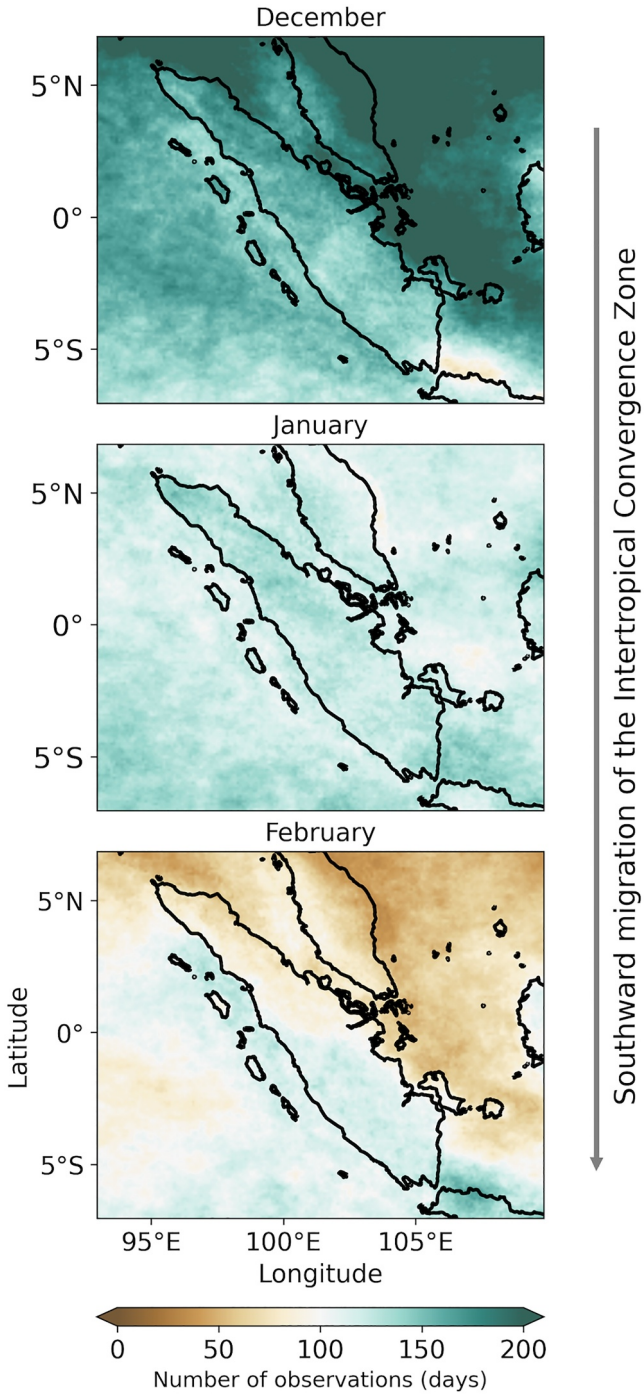


Figure 2. The maps display the number of observations with daily total precipitation exceeding the 80th percentile threshold for each month between 2001 and 2021. December is shown in the top panel, January in the central panel, and February in the bottom panel.

southern region of Sumatra. Although the selection of heavy rainfall events was only based on the PSI over land, the rainfall composite shows large regions of influence over the eastern Indian Ocean (IO) and the Malacca Strait and the connection between heavy rainfall in Sumatra and rainfall over Malaysia and Singapore. The same set of days identified as heavy rainfall days over Sumatra also contributed significantly to the total rainfall in the surrounding areas. The patterns over the surrounding seas of Sumatra may indicate local and regional sources driving severe weather in Sumatra at different scales. Examination of the fraction of the seasonal contribution of heavy rain that occurred in each month shows different temporal patterns (Figure 1b for December and Figure 1c for January and Figure 1d for February). These panels display how the seasonal contribution of heavy rainfall is distributed between individual months. Areas with values around ~25% in January are located primarily over central and northern Sumatra, the IO, and the internal seas of the MC. February shows the lowest fraction of seasonal heavy rain in Sumatra (Figure 1d), suggesting that a proportion of rainfall in that month may not be associated with heavy or large-scale island rainfall events. This indicates that the mechanisms driving austral summer heavy rainfall vary from month to month, as would be expected due to the seasonal migration of the Intertropical Convergence Zone.

3.2. Seasonal Migration of Rainfall in Sumatra

As noted, a seasonal shift of heavy rainfall occurs from December to February southward during the austral summer. To verify the mean seasonal effects and how the storm environment migrates from the Northern to Southern Hemisphere in Sumatra, the number of observations with daily total precipitation exceeding the 80th percentile (fP_{80}) threshold was calculated using IMERG data for 20 years. Figure 2 shows the monthly evolution of the frequency of fP_{80}. The maximum frequency is in December over the northern region of Sumatra and the internal seas of the MC and the eastern IO. January shows a homogeneous distribution in both hemispheres slightly increasing near the southeastern coast of Sumatra and the Java Sea. A seasonal shift occurs in February in the northern region of Sumatra; the maximum is located in the southern region and offshore Sumatra over the eastern IO. This result is consistent with the heavy rainfall contribution shown in Figure 1. Not only does heavy rain contribute more to the total in the earlier part of the DJF season but heavy rainfall occurs on more days in the earlier part of the DJF season. This indicates that the results in Figure 1 arise through multiple events rather than the contribution of a few extremely heavy events on a small number of days.

The occurrence of MCSs associated with heavy rainfall events is influenced by the diurnal variability of atmospheric conditions such as background wind flow, moisture, static stability, and local forcing and larger-scale convective behavior driven by tropical modes, including the MJO and other convectively-coupled equatorial waves. The following section presents the results of choosing the subset of heavy rain days based on the PSI.

3.3. Intraseasonal Effects on Heavy Rainfall Events

The relationship between the large-scale enhanced rainfall and the intraseasonal variability is examined by selecting each heavy rainfall event from the PSI and classifying by MJO phases from the RMM index (Wheeler & Hendon, 2004), which uses outgoing longwave radiation (OLR) satellite observations and upper-level wind data from reanalysis data. Initially, 371 heavy rainfall events were detected based on PSI for the austral summer of DJF, 2001–2021. Two hundred ninety-

21698996, 2025, 19, Downloaded from https://agupubs.onlinelibrary.wiley.com/doi/10.1029/2025JD043493 by National Health And Medical Research Council, Wiley Online Library on [27/11/2025]. See the Terms and Conditions (https://onlinelibrary.wiley.com/terms-and-conditions) on Wiley Online Library for rules of use; OA articles are governed by the applicable Creative Commons License

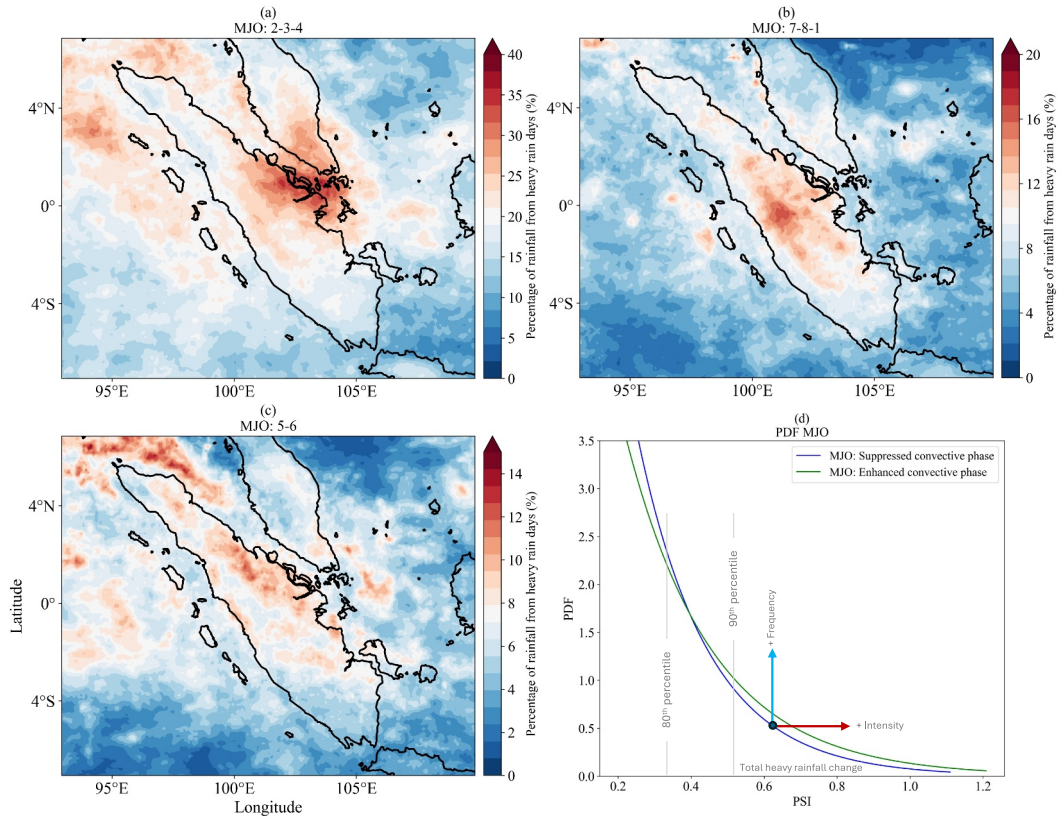


Figure 3. Composite of the percentage of heavy rainfall events to accumulated seasonal precipitation for austral summer (2001–2021) from IMERG data. (a) The MJO-enhanced convective phases (2-3-4), (b) The MJO-suppressed convective phases (7-8-1), (c) transition phases (5-6), and (d) the probability density functions (PDFs) of the PSI for two different MJO conditions over Sumatra are shown: the solid green line represents the MJO-enhanced convective phases (2-3-4), whereas the solid blue line corresponds to the MJO-suppressed convective phases (7-8-1). Please note that the color scale changes for a better representation.

four of these events occurred when the MJO amplitude ≥0.8, indicating that heavy rainfall events tend to occur during the active MJO (phase: 2-3-4, which we refer to as the MJO-enhanced convective phases over Sumatra). ∼22% of the 371 events occurred on days in phases 7-8-1 (which we refer to as the MJO-suppressed convective phases over Sumatra), and ∼63% occurs in phases 2-3-4. This result highlights the influence of the large-scale convective environment of MJO-enhanced phases on widespread heavy rainfall in Sumatra. This is different from previous results that have used composites of total rainfall with MJO phase, because our definition of widespread persistent rainfall events does not necessarily include the populations of short-lived cells that cluster around the coastlines and topography due to diurnal processes.

A common description of the enhanced convective MJO phases is that the MJO develops over the IO in phases 1 and 2, propagates eastward over the MC in phases 3 and 4, and moves away from the MC over the western Pacific in phases 5–8. Figures 3a–3c show composite analyses of the percentage of contribution of heavy rainfall events to total precipitation by the enhanced and suppressed convective phases of the MJO. In phases 2, 3, and 4, the large-scale enhanced convective envelope of the MJO moves over the western MC, and heavy rainfall contribution is higher than the MJO-suppressed convective phases over Sumatra. The dominant contribution comes from phases 2 and 3, which is also consistent with Peatman et al. (2014) and Da Silva and Matthews (2021) as shown in Figure 4. The lowlands over the east coast and the mountain ranges near the west coast of Sumatra show the highest percentage contributions of heavy rainfall (Figure 3a). The large percentage of rainfall contribution over the ocean suggests the influence of both the large-scale environment and intense coastal activities. The MJO-suppressed convective phases (phases 7-8-1) illustrate a more local signature of intense rainfall that may be linked to the diurnally forced organized convective systems over mountain ranges and the interior area of Sumatra in Figure 3b (lowland) with less connection to the rainfall contribution over the Malay Peninsula, Singapore, the

21698996, 2025, 19, Downloaded from https://agupubs.onlinelibrary.wiley.com/doi/10.1029/2025JD043493 by National Health And Medical Research Council, Wiley Online Library on [27/11/2025]. See the Terms and Conditions (https://onlinelibrary.wiley.com/terms-and-conditions) on Wiley Online Library for rules of use; OA articles are governed by the applicable Creative Commons License

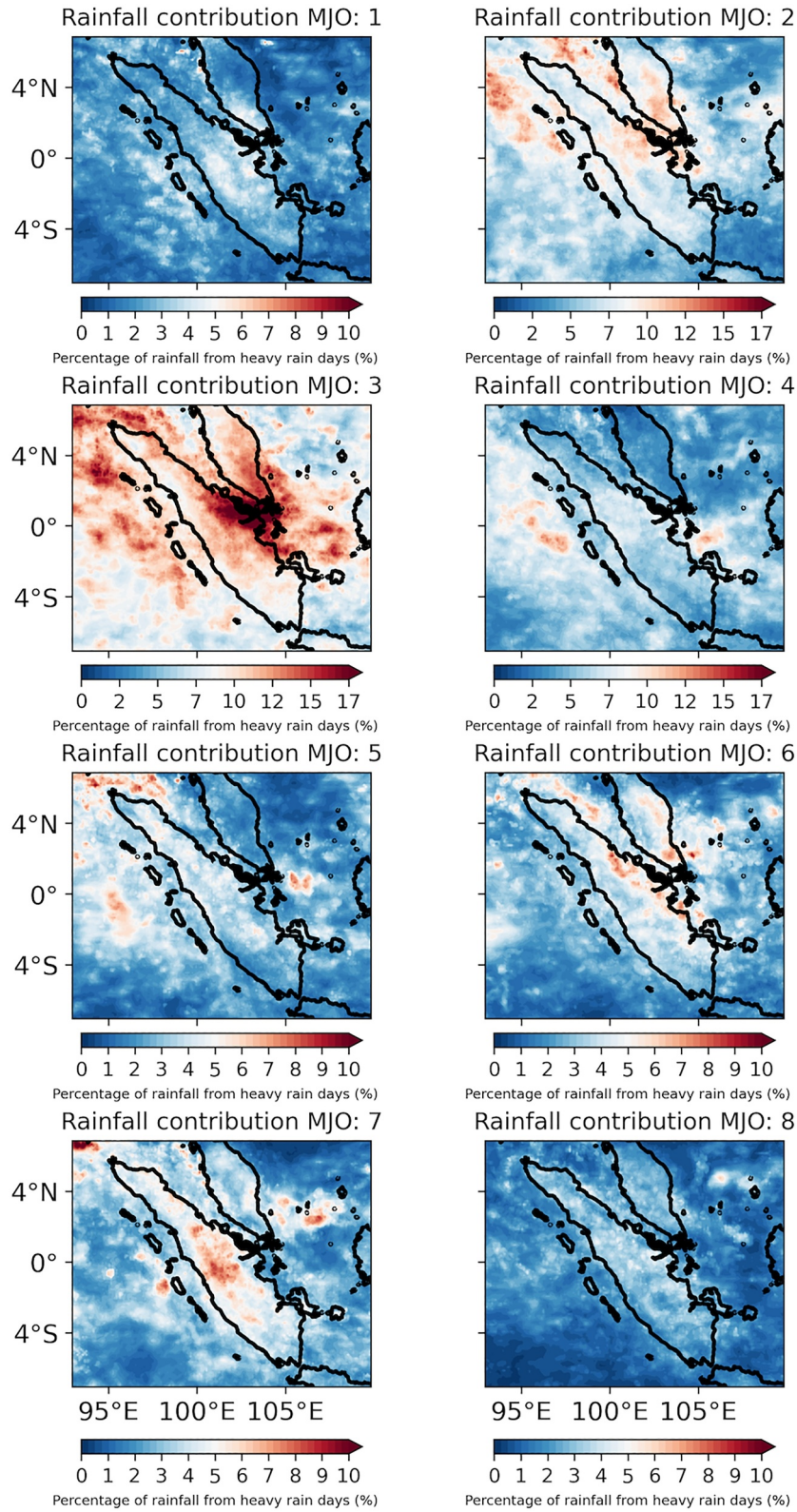


Figure 4. Composite of the percentage of heavy rainfall events to accumulated seasonal precipitation for austral summer (2001–2021) from IMERG data by MJO phases. Note that subplots of MJO phases 2, 3, and 4 have a different color palette for representation.

21698996, 2025, 19, Downloaded from https://agupubs.onlinelibrary.wiley.com/doi/10.1029/2025JD043493 by National Health And Medical Research Council, Wiley Online Library on [27/11/2025]. See the Terms and Conditions (https://onlinelibrary.wiley.com/terms-and-conditions) on Wiley Online Library for rules of use; OA articles are governed by the applicable Creative Commons License

21698996, 2025, 19, Downloaded from https://agupubs.onlinelibrary.wiley.com/doi/10.1029/2025JD043493 by National Health And Medical Research Council, Wiley Online Library on [27/11/2025]. See the Terms and Conditions (https://onlinelibrary.wiley.com/terms-and-conditions) on Wiley Online Library for rules of use; OA articles are governed by the applicable Creative Commons License

eastern IO and the internal seas of the MC. Figure 3c shows a small contribution near coastlines, lowlands, and the northern region of Sumatra that may influence storm behavior over the coastal area in the Malacca Strait as seen in MJO phase 6 (Figure 4). This result, as shown in Figure 4, expands the ratio analysis of extreme precipitation in Da Silva and Matthews (2021), showing detailed areas in Sumatra with a large influence from extreme rainfall based on MJO phases.

To illustrate how heavy rainfall varies with different MJO phases, we calculated the probability density functions (PDFs) of the PSI for both suppressed and enhanced convective phases of the MJO. Figure 3d shows that while heavy rainfall events (PSI > 0.4) occur under both conditions, they are more frequent and intense during the enhanced convective phases. This increased occurrence reflects a stronger contribution from high-intensity events, which are typically associated with more severe weather conditions during these phases.

3.4. Large-Scale Moisture Contribution and Circulation During Heavy Rainfall Events

During the MJO-enhanced convective phases, the spatial distribution of the moisture advection and convergence can be controlled by large-scale atmospheric processes (MJO: 2, 3, and 4 in Figure 5), where more moisture is transported from the IO by anomalous westerlies near the equator in the lower troposphere (925–850 hPa) associated with changes in the strengthening of large-scale circulation during the heavy rainfall events (not shown). In contrast, during the MJO-suppressed convective phases, large-scale dependency reduces due to the regional subsidence over the western MC. Vertically integrated moisture flux convergence (VIMFC) is used to underline the large-scale dynamics and moisture contribution during heavy rainfall events. Figure 5 shows the composites of VIMFC-ERA5 for each MJO phase on heavy rainfall days during the austral summer and the MJO induces more moisture convergence in phases 2, 3, and 4 over the IO, and this structure tends to be weak in phase 8. Our analysis suggests a strong equatorial zonal moisture flux convergence in the western MC. The strength of convective activity associated with each MJO phase varies as it propagates across the MC. However, the composites of VIMFC suggest an intense moisture convergence over the mountain ranges of Sumatra and coastal areas during the heavy rainfall days for all MJO phases. The VIMFC also show a variety of patterns over the IO and the internal seas of the MC. This convergence is especially pronounced over the coastal areas and orographic regions of Sumatra where topographic lifting enhances moisture accumulation. These persistent and intense VIMFC areas provide favorable conditions for the initiation and maintenance of deep convection, which are key ingredients for the development of MCS.

Figure 6 shows the composite pattern of VIMFC anomalies for all heavy rainfall events identified using the PSI with MJO phases defined by RMM index amplitudes ≥0.8. The baseline was calculated for all days with RMM amplitudes ≥0.8 in each MJO phase from 2001 to 2021. The dots in Figure 6 indicate anomalies statistically significant at the 95% confidence level. Significant anomalies are located throughout Sumatra and its surrounding seas (Dotted in Figure 6), and the northward extension of the positive anomaly of the VIMFC (Reanalysis, ERA5) is consistent with the percentage of seasonal rainfall associated with heavy events in Figure 1 (Satellite-based rainfall, IMERG). To understand the role of the MJO in providing moisture to the region, events with an amplitude of the RMM index <0.8 were selected to produce a VIMFC composite. The results suggest that these events are associated with weaker VIMFC anomalies over Sumatra (Figure S2 in Supporting Information S1) in contrast to the more intense anomalies observed during events with MJO amplitude ≥0.8. This result supports the idea that MJO plays a key role in enhancing moisture transport and convergence over the region during heavy rain days. However, the findings also indicate that, regardless of the MJO phase or its convective contribution, a sufficiently strong anomaly in large-scale moisture flux is still necessary to trigger widespread heavy rainfall particularly when acting in conjunction with local forcings.

Figure 7 shows the composite mean 925–850 hPa streamlines and relative vorticity anomalies during heavy rainfall events for each MJO phase. Four dominant circulation regions can be identified: (a) a seasonal cyclonic circulation north of Sumatra and over the eastern IO, whose strength depends on the magnitude and incidence angle of background flow from the central region of the MC and the angle of incidence of the flow on the mountain ranges in the Malay Peninsula, producing a downstream vorticity maximum in northern Sumatra (Hardy et al., 2023; Koseki et al., 2014). (b) A semipermanent low-level vortex west of Borneo, which promotes low-level convergence and cyclonic circulation over south-central Sumatra (Fine et al., 2016). (c) The Australian monsoon circulation forms a second center of cyclonic vorticity in the equatorial southern IO during MJO phases 1–3. This offshore vortex south of Sumatra is favored by both easterly and westerly low-level flows interacting

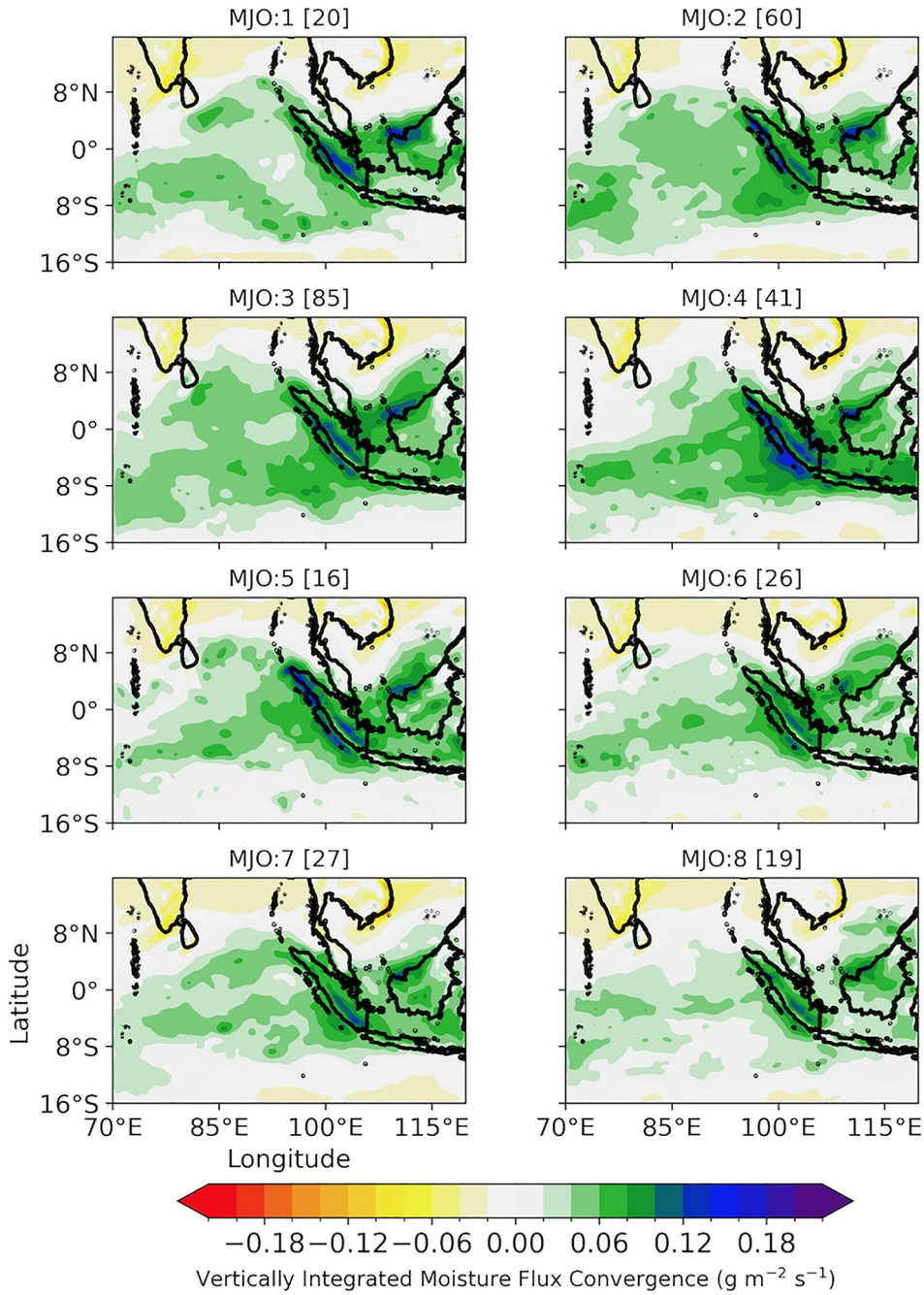


Figure 5. Composite of vertically integrated moisture flux convergence (VIMFC; g m^{-2} s^{-1}) from ERA5 for MJO phases 1–8 during the austral summer. Composites are based on heavy rainfall days identified using the Precipitation Severity Index (PSI) with active MJO phases defined by the RMM index (amplitude ≥0.8). The number of heavy rainfall days is indicated in brackets for each MJO phase.

with the mountain ranges in Sumatra (See the blue stars in panel MJO phase 2 of Figure 7) consistent with previous work showing that mountain-induced flow blocking and splitting are key drivers of wake vortex formation with additional modulation by MJO phase (Fine et al., 2016; Johnson et al., 2023). (d) The enhanced convective phases of the MJO over the equatorial IO (phases 2–4, not shown) and the complex interactions when its cloud envelope reaches the MC.

21698996, 2025, 19, Downloaded from https://agupubs.onlinelibrary.wiley.com/doi/10.1029/2025JD043493 by National Health And Medical Research Council, Wiley Online Library on [27/11/2025]. See the Terms and Conditions (https://onlinelibrary.wiley.com/terms-and-conditions) on Wiley Online Library for rules of use; OA articles are governed by the applicable Creative Commons License

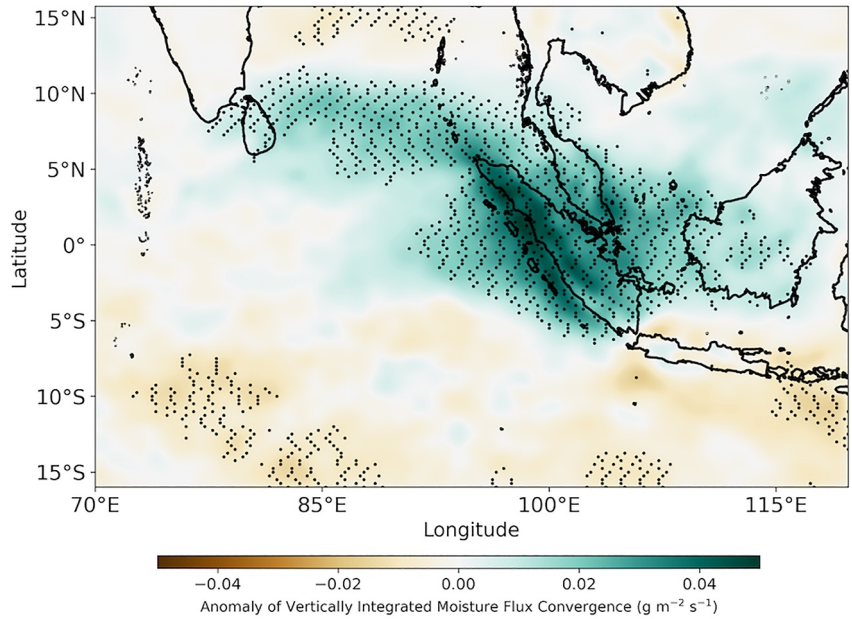


Figure 6. Composite anomalies of vertically integrated moisture flux convergence (VIMFC; g m^{-2} s^{-1}) from ERA5. Composite of VIMFC for all heavy rain and MJO for the austral summer. Heavy rain days were chosen using the PSI and MJO phases given by the RMM index with amplitude ≥0.8. The baseline was calculated for all days with RMM amplitudes ≥0.8 in each MJO phase from 2001 to 2021. Dots indicate statistically significant at the 95% level of VIMFC anomalies.

The interplay between westerly flow over the eastern IO and northeasterly flow over the internal seas of the MC, modified by blocking and splitting around the mountain ranges of Sumatra, plays an important role in shaping cyclonic vorticity patterns in the internal seas of the MC and intensifying rainfall over Sumatra. Upstream blocking of equatorial westerlies contributes to cyclonic circulations in both hemispheres, whereas positive relative vorticity anomalies in the Java Sea can combine with these terrain-induced effects to further enhance heavy rainfall events. The composites for heavy rain days also reveal that MJO phases 5 to 8 exhibit a positive anomaly along with equatorial westerlies in the eastern IO. This phenomenon can be attributed to the propagation of convectively coupled Kelvin waves as noted by Fine et al. (2016).

3.5. Diurnal Variations During Heavy Rainfall Events in Sumatra

The diurnal rainfall variations in Sumatra and associated offshore propagating rainfall signatures have been well established in several studies (Bai et al., 2021; Lopez-Bravo et al., 2023a, 2023b; Mori et al., 2004; Peatman et al., 2023; Sakaeda et al., 2020; Short et al., 2019; Vincent & Lane, 2016; Wei et al., 2020; Wu et al., 2008). However, the previous works have not evaluated particularly the diurnal evolution of heavy rainfall over Sumatra. To address this gap, we apply a hierarchical clustering technique to spatially averaged rainfall over land for each heavy rainfall day identified by the PSI. This approach differs from previous studies by explicitly characterizing the timing and magnitude of rainfall accumulation over land during heavy rainfall days rather than focusing on average diurnal cycle of rainfall (Da Silva & Matthews, 2021; Vincent & Lane, 2017). Note that these are specifically clusters of heavy rainfall events, and diurnal variations can be driven by large-scale conditions. Sometimes, the diurnal cycle is enhanced, for example, the MJO enhances the diurnal cycle of rainfall and clouds (Lopez-Bravo et al., 2023b; Peatman et al., 2014, 2023). Other times, the diurnal cycle is modified, for example, in the presence of a CCKW, as found by Senior et al. (2023).

Six clusters of the average rainfall over time are identified during heavy rainfall events over land in Sumatra. Figure 8a shows the average rainfall of the events in each cluster. The average rainfall has been normalized by the maximum spatially averaged rainfall in phase 5. Figure 8b displays the relative frequency of the maximum rainfall time for each cluster, indicating how often the peak rainfall occurs at each hour expressed as a fraction of the total number of heavy rainfall days classified within that cluster. The most frequent rainfall pattern (cluster 4, 194 events) corresponds to the diurnal precipitation cycle with a maximum of rain between 17:00 (LST, UTC+7

21698996, 2025, 19, Downloaded from https://agupubs.onlinelibrary.wiley.com/doi/10.1029/2025JD043493 by National Health And Medical Research Council, Wiley Online Library on [27/11/2025]. See the Terms and Conditions (https://onlinelibrary.wiley.com/terms-and-conditions) on Wiley Online Library for rules of use; OA articles are governed by the applicable Creative Commons License

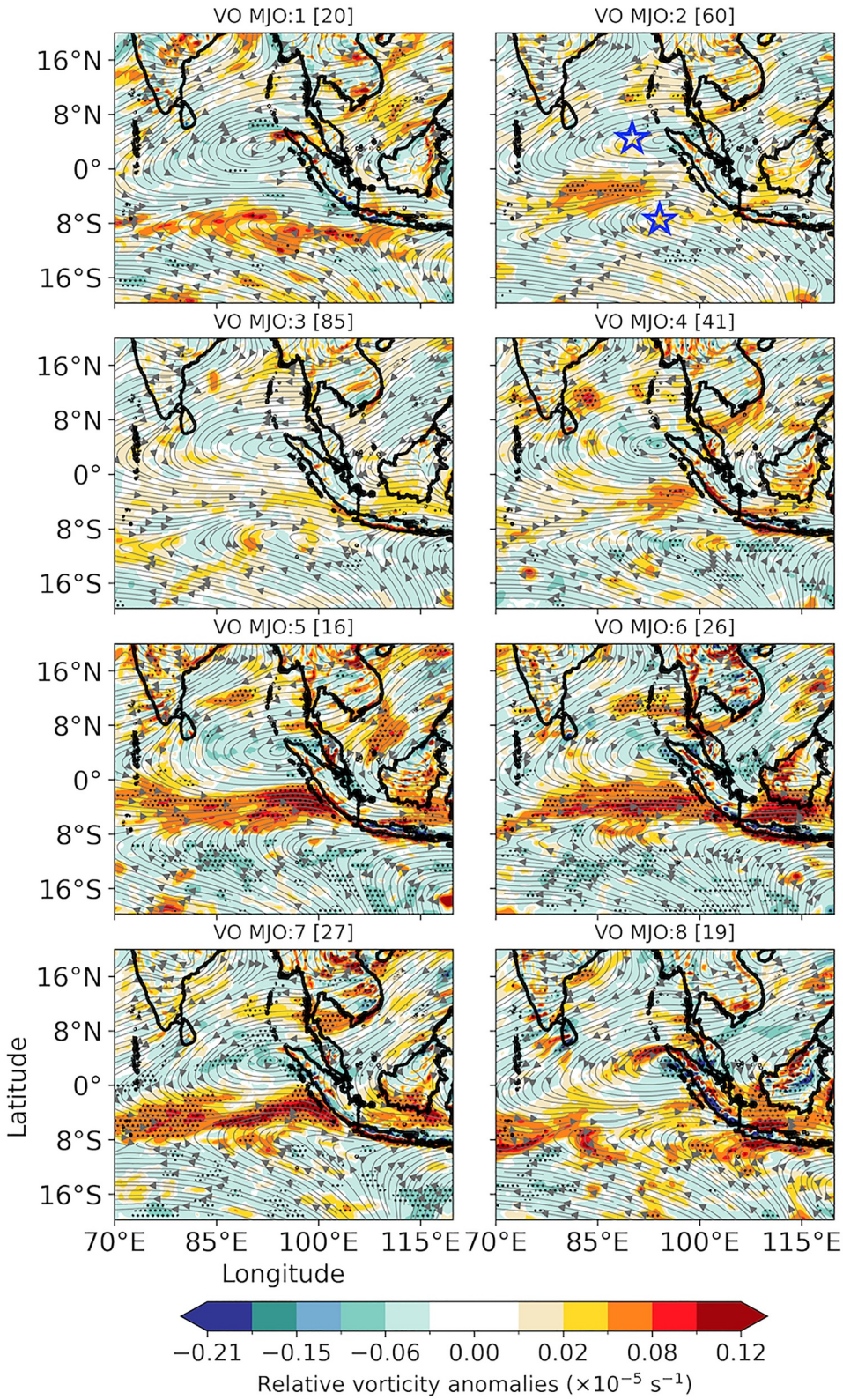


Figure 7. Composite mean 925–850 hPa streamlines (arrows) and relative vorticity anomalies (shading, $\times 10^{-5}$ s^{-1}) for heavy widespread rainfall events during the austral summer conditionally averaged by MJO phase (amplitude ≥0.8). The baseline was calculated for all days with RMM amplitudes ≥0.8 in each MJO phase from 2001 to 2021. The number of heavy rainfall days is indicated in brackets for each MJO phase and the blue stars in MJO phase 2 indicate the location of the twin vortex over the Indian Ocean. Dots indicate statistically significant at the 95% level of relative vorticity anomalies.

21698996, 2025, 19, Downloaded from https://agupubs.onlinelibrary.wiley.com/doi/10.1029/2025JD043493 by National Health And Medical Research Council, Wiley Online Library on [27/11/2025]. See the Terms and Conditions (https://onlinelibrary.wiley.com/terms-and-conditions) on Wiley Online Library for rules of use; OA articles are governed by the applicable Creative Commons License

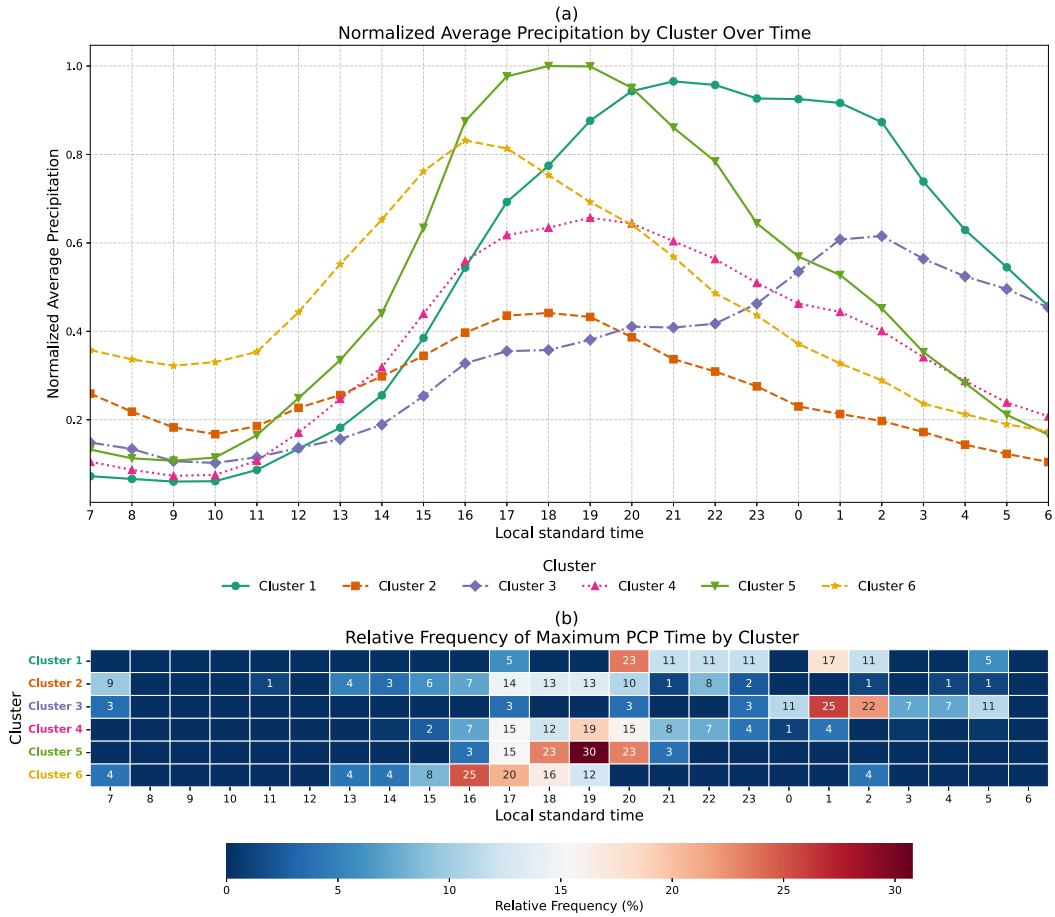


Figure 8. Cluster analysis of hourly accumulated rainfall over land in Sumatra during heavy rainfall events. The *Y*-axis shows the normalized cluster average of accumulated precipitation over land in Sumatra, and the *X*-axis indicates the local standard time in Sumatra (LST, UTC+7 for Sumatra). (a) Normalized average precipitation: each line represents the average accumulated rainfall for the number of events within each cluster category. The average rainfall has been normalized using the maximum rainfall cluster over time. (b) The heat map shows the relative frequency of the maximum rainfall time for each cluster calculated as the proportion of heavy rainfall events on which the maximum rainfall occurs at a given hour relative to the total number of heavy rain days within each cluster. The colors on the *Y*-axis match the colors in the legend of panel (a). The events were identified using the PSI derived from IMERG V6. Period: 2001–2021; Method: Hierarchical clustering.

for Sumatra) and 21:00 LST and decreases toward the morning hours. Cluster 5 (26 events) exhibits a diurnal pattern similar to Cluster 4 with an increased amount of rainfall, and the maximum peak is recorded at 19:00 LST (Figure 8b). Cluster 2 (83 events) also shows an evident diurnal rainfall variation peaking between 17:00 LST and 20:00 LST with a rainfall reduction over Sumatra relative to clusters 4 and 5. However, the main difference is the early peak of rainfall at 07:00 LST, which can explain an accumulative effect linked to a rainfall event of the previous day or early in the morning of the diurnally forced rainfall. In contrast, cluster 1 (17 events) shows that rainfall peaks after 20:00 LST with a persistent amount of rainfall during the night, indicating that the time window of the maximum peak of rainfall increases. This can indicate persistent rainfall and the extended lifetime of storms associated with MCSs. The persistence effect is also observed in cluster 3 (27 events). A cumulative effect can be observed with developing rainfall from 00:00 UTC (07:00 LST). Some heavy rainfall events exhibit a relative maximum at 17:00 LST (not shown) to finally peak around 01:00 LST, showing the nighttime diurnal regime of heavy rainfall and the bimodal signature of the diurnal cycle in Sumatra (Lopez-Bravo et al., 2023b). Finally, Cluster 6 (24 events) indicates an early peak rainfall between 15:00 LST and 19:00 LST and decreases during the afternoon. These results are consistent with Vincent and Huang (2022), who showed that the morning incoming shortwave radiation could modulate both the timing and amplitude of the afternoon rainfall peak. These

21698996, 2025, 19, Downloaded from https://agupubs.onlinelibrary.wiley.com/doi/10.1029/2025JD043493 by National Health And Medical Research Council, Wiley Online Library on [27/11/2025]. See the Terms and Conditions (https://onlinelibrary.wiley.com/terms-and-conditions) on Wiley Online Library for rules of use; OA articles are governed by the applicable Creative Commons License

Table 1
Number of Days in Each MJO Phase-Himawari-8 AHI for DJF and Amplitude ≥0.8

Phase	Number of days
1	4
2	19
3	22
4	20
5	9
6	7
7	3
8	8

results show that even though island-scale rainfall events require the support of the large-scale environment, they still exhibit a strong diurnal cycle.

3.6. Cloud Top Properties During Heavy Rain Events

Although intraseasonal variability plays an important role in promoting large-scale convection over the western region of the MC, the heavy rainfall events also depend on the day-to-day variations of wind and moisture that drive the cloud distributions over the eastern IO and the MC under both MJO-enhanced or suppressed conditions. However, cloud populations over Sumatra are also associated with organized mesoscale convective systems with a pronounced temporal variability during the austral summer. In this section, the analysis has been limited to the Himawari-8 AHI era (Six austral summers-DJF: 2016–2021) to explore the multicell environment of diurnally driven convection during heavy rainfall events in Sumatra.

Movie S1 shows the diurnal variations of cold cloud regions based on the brightness temperature of the 10.4 μm spectral band from Himawari-8 AHI data covering latitude 16°S–10°N and longitude 83°E–115°E with 2 km spatial and 1-hourly temporal resolution. The PSI has been used to select dates associated with heavy rainfall events in Sumatra, identifying 92 days as heavy rainfall events during the austral summers 2016–2021. Table 1 presents the number of days by phase of the MJO. Note that the highest frequencies occur in the enhanced convective phase of the MJO. Despite the limited samples, geostationary data have been used to explain the features of mesoscale systems associated with heavy rainfall events. First, the 10th percentile of $BT_{10.4}$ shows the coldest region over the western region of the MC (green and blue colors in Movie S1). This result highlights the large-scale effect over the cold cloud top distribution regionally at the intraseasonal scale with large cold areas during the enhanced convective phase of the MJO (MJO: 2, 3, and 4). However, the coldest areas show sub-structures embedded into the large-scale convective envelope, which are linked to diurnally driven convection over the major islands of the MC and the Malay Peninsula. These substructures have been identified by Nakazawa (1988) and discussed by Kiladis et al. (2009) showing that the MJO often has embedded within several species of eastward and westward propagating waves, including Convectively coupled Kelvin waves and propagating inertio-gravity waves. In contrast, the diurnally driven convection controls the cloud population distribution during the suppressed convective phase of the MJO (MJO: 7, 8, and 1). Additionally, the local diurnal signatures of cold cloud tops indicate a large variability of deep convective structures consisting of multiple cold cloud cores as is proposed by Feng et al. (2021) and Lopez-Bravo et al. (2023a). These cores frequently propagate both offshore and onshore over Sumatra during heavy rainfall events. For example, inland propagation observed during MJO phase 8 in Movie S1.

3.7. Heavy Rainfall Events and Cold Cloud Area and Cold Cloud Core

We hypothesize that embedded convective cold cores within extensive cold cloud shields are a primary driver of heavy rainfall over Sumatra. The formation, intensity, and organization of these cores are modulated by diurnal variability and large-scale MJO-related atmospheric conditions. Although these cold cores generally control rainfall patterns, heavy rainfall can occasionally occur even with fewer convective cold cores, reflecting contributions from mesoscale and large-scale circulations. To explore this hypothesis, the cold cloud area and cold cloud core area were detected separately in every hourly Himawari-8 scene over the 6 years of DJFs. Figure 9 shows an example of the cold cloud area and cold cloud core identification over Sumatra. The $BT_{10.4}$ associated with a heavy rainfall event is indicated by the gray shading in Figure 9; the green and yellow shaded indicate the cold cloud area and cold cloud core, respectively.

Figure 10 presents the mean diurnal cycle of cold cloud areas and cold cloud core areas over land in Sumatra during the Himawari-8 AHI period. The analysis compares all days during the austral summer (DJF; 532 days, 2016–2021) with heavy rainfall days (92 days, 2016–2021) identified using PSI and IMERG data. The orange and light blue lines represent the average over all DJF seasons, whereas the red and blue lines indicate composites for heavy rainfall events. Shaded regions denote the 95% confidence intervals. The results show that the total cold cloud area and the cold cloud core area increase during heavy rainfall events compared to the seasonal average, indicating a larger cloud area of deeper and colder convective clouds. The increase in cold core areas suggests

21698996, 2025, 19, Downloaded from https://agupubs.onlinelibrary.wiley.com/doi/10.1029/2025JD043493 by National Health And Medical Research Council, Wiley Online Library on [27/11/2025]. See the Terms and Conditions (https://onlinelibrary.wiley.com/terms-and-conditions) on Wiley Online Library for rules of use; OA articles are governed by the applicable Creative Commons License

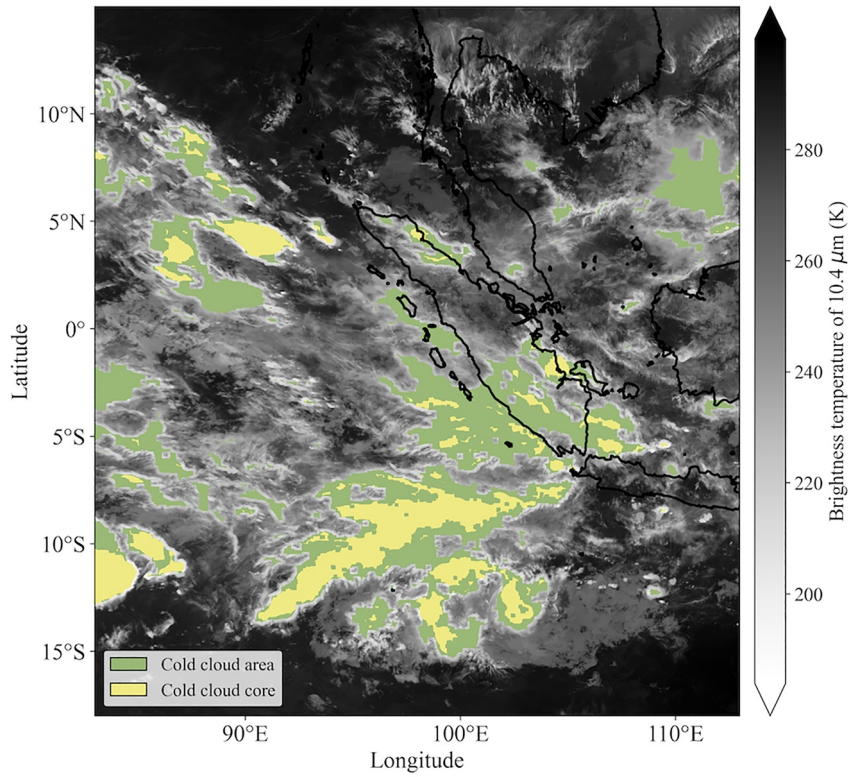


Figure 9. The brightness temperature of 10.4 μm (K) in shaded gray at 05:00 LST 12 January 2021. The green and yellow shaded indicate the cold cloud area (240 K) and cold cloud core (213 K), respectively. Data from Himawari-8 AHI.

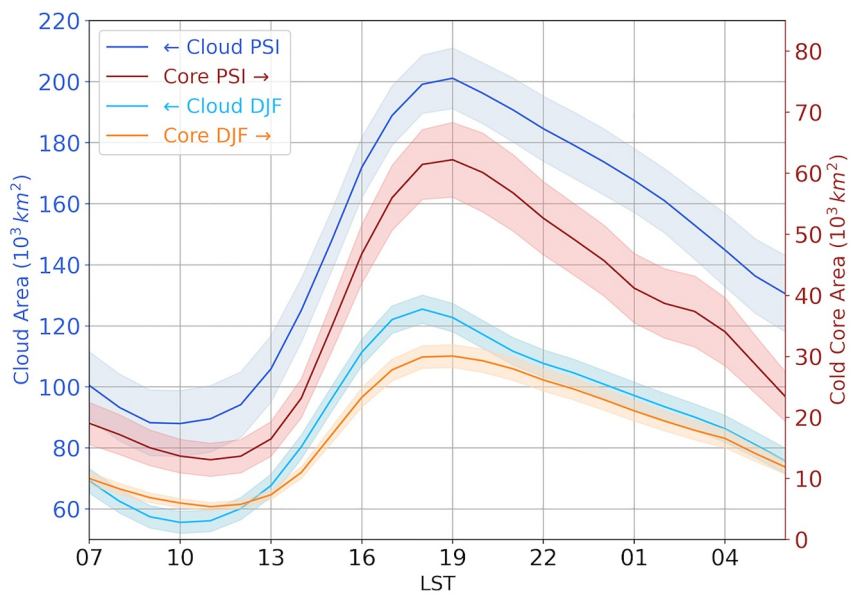


Figure 10. Analysis of cold cloud tops over land Sumatra derived from Himawari-8 AHI brightness temperature channel 13 over six austral summers (2016–2021). The average cold cloud area (left *y*-axis, 10^3 km^2) for DJF is shown in the solid light blue line, whereas the average cold cloud area during heavy rainfall events in DJF is shown in the solid dark blue line. The average cold cloud core area (right *y*-axis, 10^3 km^2) is shown in the solid orange line for the seasonal mean and the solid red line for heavy rainfall events in DJF. Color-shaded areas indicate the 95% confidence interval for the weighted mean.

21698996, 2025, 19, Downloaded from https://agupubs.onlinelibrary.wiley.com/doi/10.1029/2025JD043493 by National Health And Medical Research Council, Wiley Online Library on [27/11/2025]. See the Terms and Conditions (https://onlinelibrary.wiley.com/terms-and-conditions) on Wiley Online Library for rules of use; OA articles are governed by the applicable Creative Commons License

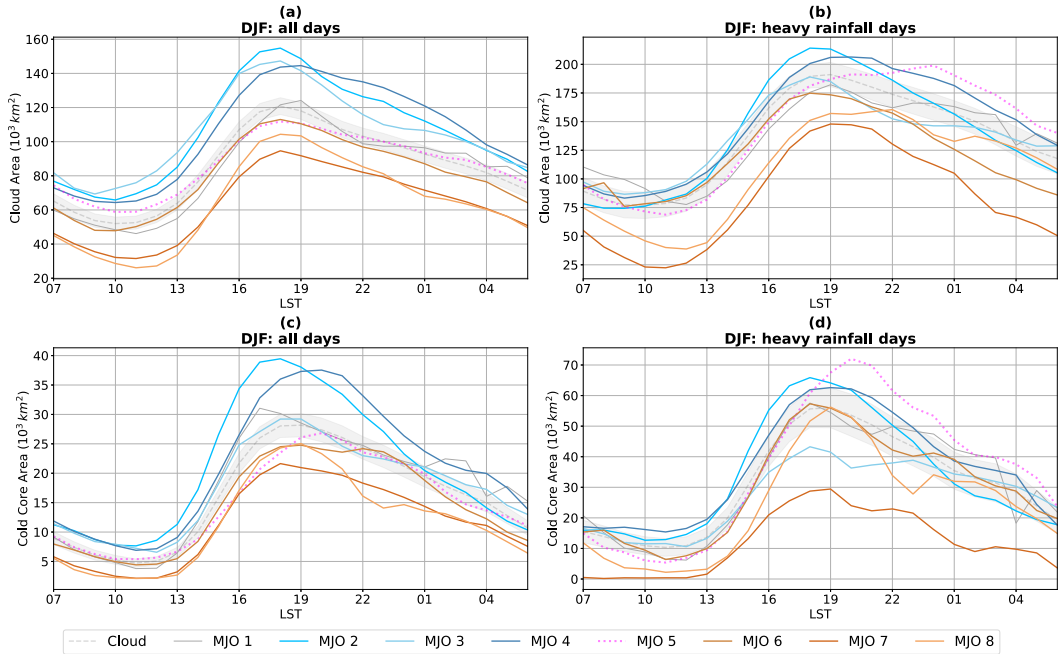


Figure 11. Analysis of cold cloud tops based on brightness temperature channel 13 from Himawari-8 AHI. (a) Cold cloud Area (*Y*-axis, 10^3 km^2) for six austral summers (DJF, 2016–2021). Dashed gray line shows the mean for all MJO phases: (2016–2021) and color lines display the averages for each MJO phase and LST bin. (b) As panel (a) for heavy rainfall events. (c) cold cloud core (*Y*-axis, 10^3 km^2) for six austral summers (DJF, 2016–2021). Dashed gray line shows the mean for all MJO phases: (2016–2021). (d) As panel (c) for heavy rainfall events. The blue color lines indicate the active phases of the MJO (2-3-4), and the warm colors display the inactive phases of the MJO (6-7-8). The black solid line represents MJO Phase 1, whereas MJO Phase 5 is shown by the dotted magenta line. Color-shaded areas indicate the 95% confidence interval for the weighted mean across MJO phases for the cloud area and cloud core area at each LST. Note different *y*-axis for representation.

stronger convective updrafts, whereas the observed delay in the diurnal peak indicates shifts in convective organization and timing. Together, these changes support a link between heavy rain and the presence of more organized deep convection over Sumatra.

Figure 11 extends this analysis by decomposing the diurnal cycle by MJO phase (for MJO amplitude ≥ 0.8). This decomposition reveals significant variations in cloud coverage patterns in different phases, reflecting the influence of large-scale intraseasonal variability on convective organization. Differences in diurnal signatures between seasonal mean and heavy rainfall composites further indicate contributions from multiple scales of variability, including mesoscale convective systems and a broader modulation of MJO.

The relative prevalence of cold cloud areas and cold cloud cores is expected to strongly reflect the transition from locally forced convection during the MJO-suppressed convection phases to large-scale background convection during the MJO active phases. Figure 11 reveals a number of relevant points about the relative occurrence of cold cloud areas and cold cloud cores. Considering all DJF days within 6 years (Figures 11a and 11c), there is an expected increase in the cold cloud areas during the convectively active phases of the MJO: 2-3-4. The cold cloud cores follow almost the same pattern on all days with the notable exception of phase 3 (Figure 11c), which shows a decrease in the cold cloud core areas. This is consistent with the large-scale envelope of the MJO that supports the intraseasonal rainfall pattern for all days in cold cloud areas (Figure 11a) and cold core areas (Figure 11c).

A more complex story emerges when considering only the heavy rainfall days within the period (Figures 11b and 11d). Similar to the result for all DJF days, there is a decrease in the cold cloud cores in phase 3 (Figure 11d), indicating that heavy rainfall is occurring despite a small number of cold cloud cores. Figure 11d shows a maximum cold cloud core area during heavy rainfall events in the transitional phase between the convective and the MJO-suppressed convection phase 5 over Sumatra. This signature corresponds to Cluster 1 in Figure 8 where 88% of heavy rainfall days occur in that phase. This supports our interpretation that the peak in cold cloud core area in MJO Phase 5 reflects locally forced convection; in this phase, the large-scale convective environment is

21698996, 2025, 19, Downloaded from https://agupubs.onlinelibrary.wiley.com/doi/10.1029/2025JD043493 by National Health And Medical Research Council, Wiley Online Library on [27/11/2025]. See the Terms and Conditions (https://onlinelibrary.wiley.com/terms-and-conditions) on Wiley Online Library for rules of use; OA articles are governed by the applicable Creative Commons License

21698996, 2025, 19, Downloaded from https://agupubs.onlinelibrary.wiley.com/doi/10.1029/2025JD043493 by National Health And Medical Research Council, Wiley Online Library on [27/11/2025]. See the Terms and Conditions (https://onlinelibrary.wiley.com/terms-and-conditions) on Wiley Online Library for rules of use; OA articles are governed by the applicable Creative Commons License

dominated by the MJO-suppressed convection phases over Sumatra, and convection is primarily initiated by land and sea breezes. In phase 7 (Figure 11d), we see a decrease in the peak cold cloud cores area during heavy rainfall events, indicating that heavy rainfall may occur in this phase outside of the context of widespread cold cloud cores. The reason for this is not immediately obvious but may be related to some aspect of the large-scale circulation, as we note higher levels of relative vorticity to the north of Sumatra in this phase relative to the other suppressed convective phases.

4. Discussion

This study aimed to examine the contribution of widespread, persistent rainfall to the total rainfall climate in Sumatra and to relate this rainfall to the MJO and the cloud morphology. Large-scale precipitation is influenced by the intraseasonal variability itself, moisture transport, and large-scale circulation patterns, whereas locally forced precipitation is influenced by surface forcing, topographic forcing, microphysics, column moisture, and local convergence patterns, although we acknowledge that these factors are not isolated from one another.

By examining the rainfall in the region around Sumatra on days that had been identified as heavy island-scale rainfall days, it is shown that in the convectively active phases (phase 2-3-4), heavy rainfall over Sumatra is part of the larger-scale envelope of the MJO. In phase 7, 8, and 1, heavy rainfall days over Sumatra do not occur concurrently with heavy rainfall days in the wider region, indicating a more local forcing. These results were linked to the cloud top temperature observations: In phase 3, there is a minimum in the relative area of cold cloud cores to cold cloud areas on days of heavy rainfall, indicating that on these days, cold cloud cores may play a lesser role in producing island-scale heavy rainfall likely related to rainfall within MCS with embedded cores. In phase 7, there is also a minimum in the relative area of cold cloud cores, but in this case there is much less rainfall overall over Sumatra, little connection to regional precipitation, and also less cloud overall. This likely represents less vigorous convection and less convective development.

The dual analysis of heavy island-scale rainfall and cloud tops uniquely links the spatial distribution and intraseasonal variability of rainfall to the type of convection underpinning the rainfall. This supports the argument that modeling rainfall extremes and intraseasonal rainfall variability in the tropics may require convective-permitting modeling approaches even when the precipitation is aggregated to island-scale.

Combining satellite-based precipitation from IMERG, cloud top features from Himawari-8 AHI, and reanalysis data have allowed us to explore the processes driving heavy rainfall events. This includes their local diurnal convective signatures in both rainfall and cold cloud tops, which are modulated by the intraseasonal-scale variability over Sumatra. However, this study only examined heavy rainfall events using remote sensing products. Ground-based precipitation observations were not included due to the lack of available data, and gridded precipitation, products such as the Asian Precipitation-Highly-Resolved Observational Data Integration Towards Evaluation of Water Resources were not homogeneous for a long-term analysis over Sumatra. This is a limitation of the current study because satellite-based precipitation products are subject to large uncertainties in the estimates of rainfall intensity and location of rainfall patterns (Tan et al., 2019; Tapiador et al., 2020; Watters et al., 2021). Previous studies have also identified a time lag in the maximum peak of diurnal precipitation of ∼1 hr in the IMERG data set (Tan et al., 2019; You et al., 2019). This data set gives a well-resolved representation of deep convective clouds, which is relevant over land in Sumatra because, for a 2-day time scale, we assume most rainfall comes from deep convective clouds. This approach may be less relevant in areas where a high proportion of the total precipitation comes from, for example, marine stratocumulus clouds.

Identifying organized and intense rainfall events and diurnally forced convection as an essential element of the tropical water cycle offers an opportunity to understand the role of organized convection from mesoscale convective systems in heavy precipitation in the MC. Our results suggest that heavy rainfall events contribute significantly to seasonal rainfall during the austral summer DJF in Sumatra. This finding is consistent with that of Peatman et al. (2014), Vincent and Lane (2016), Schumacher and Rasmussen (2020), Da Silva and Matthews (2021), Latos et al. (2021), and Crook et al. (2024) who have discussed the importance of mesoscale convective systems in tropical extreme-precipitation events and their role as a critical component of the hydrologic cycle.

We also show that the seasonal signature of intense rainfall frequency explains the local meridional variation associated with the annual migration cycle of the Intertropical Convergence Zone (ITCZ) and the impact on storm

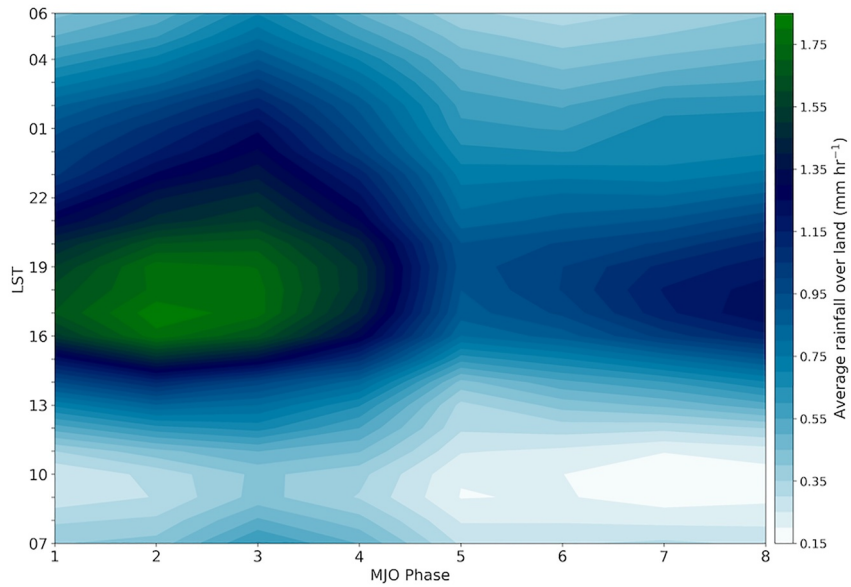


Figure 12. Average austral summer variation in rainfall with time of day and MJO phase for 2001–2021 from IMERG data similar to Peatman et al. (2014) and Vincent and Lane (2017).

distribution during summer. This is consistent with Sakurai et al. (2005), who studied changes in the diurnal propagation regimes and transition times of the cloud populations due to wind variations in the lower troposphere linked to the annual migration of the ITCZ. These results also agree with Kerns and Chen (2018) and Peatman et al. (2023), who provide evidence of the DJF seasonal rainfall and how persistent stronger winds and continuous convergence produce intense night-morning precipitation by the migration of the ITCZ. Additionally, six predominant diurnal regimes of heavy rainfall over land in Sumatra reflect prerainfall conditions. These patterns are characterized by various aspects of rainfall, including timing, intensity, persistence, duration, and spatial extent. These characteristics are derived from a cluster analysis conducted prior to the peak of the rainfall, which indirectly indicates different environmental conditions.

The effects of intraseasonal-scale variability on the contribution of heavy rainfall events to total daily rainfall have been highlighted in our investigation. This is an important finding in understanding the spatial distribution of the percentage of rainfall linked to heavy rainfall by MJO phases with the highest contribution in the MJO phases 2, 3, and 4. The findings are directly in line with previous results by Oh et al. (2012), Peatman et al. (2014), and Yokoi et al. (2017), who found that a dominant offshore wind produces a typical diurnal cycle signature with intense and deep convection over the land and coastal regions. This increases the probability of heavy rainfall events due to changes in the diurnally driven convection in Sumatra with the induced largest diurnal amplitude occurring ahead of the propagating convective envelope of MJO as has been explained by Peatman et al. (2014), Birch et al. (2016), and Vincent and Lane (2016, 2017). However, these studies have uniquely considered the rainfall intensity to conclude that extreme/heavy rainfall is more intense in MJO phase 2, as shown in Figure 12, which reproduces earlier work of Peatman et al. (2014) and Vincent and Lane (2017) but with high resolution data from IMERG. Our analysis has shown that although phase 2 shows the strongest rainfall intensity in mean conditions, the occurrence of rainfall events with a weaker intensity is more significant in phase 3 of the MJO, which is reflected in the accumulated seasonal rainfall signature. In contrast, the suppressed convective phase of the MJO showed inland contributions. This result agrees with Vincent and Lane (2016) and Vincent and Huang (2022), who explore the influence of large-scale moisture variations in controlling afternoon-night diurnal rainfall in Sumatra, which this study suggests is also relevant during heavy rainfall events.

From a broader perspective, understanding the evolution of heavy rainfall over land in Sumatra under the enhanced and suppressed convective phases of the MJO is directly related to the evolution of mesoscale convective systems and the multiscale interaction of the diurnally driven convection. The results demonstrate: first, the complex developments of cold cloud populations by MJO phases due to nonlocal features over the western region of the MC. The large-scale variability shown here in the eastern IO is consistent with studies by

21698996, 2025, 19, Downloaded from https://agupubs.onlinelibrary.wiley.com/doi/10.1029/2025JD043493 by National Health And Medical Research Council, Wiley Online Library on [27/11/2025]. See the Terms and Conditions (https://onlinelibrary.wiley.com/terms-and-conditions) on Wiley Online Library for rules of use; OA articles are governed by the applicable Creative Commons License

21698996, 2025, 19, Downloaded from https://agupubs.onlinelibrary.wiley.com/doi/10.1029/2025JD043493 by National Health And Medical Research Council, Wiley Online Library on [27/11/2025]. See the Terms and Conditions (https://onlinelibrary.wiley.com/terms-and-conditions) on Wiley Online Library for rules of use; OA articles are governed by the applicable Creative Commons License

Salby and Hendon (1994), Maloney and Hartmann (1998), Matthews (2000), Peatman et al. (2014, 2021), and Baranowski et al. (2016). These earlier studies proved how the changes in moisture convergence and induced wind anomalies from large-scale circulation can drive the cloud variability over the MC, thereby affecting the diurnally driven convection over the major islands of the MC during the MJO phases. Second, organized mesoscale convective systems are key to shaping the characteristics of heavy rainfall over inland Sumatra. Here, the unprecedented high-resolution geostationary observations from Himawari-8 AHI make it possible to characterize cloud top features to investigate the diurnally driven convection in Sumatra, building on the recent studies by (Lopez-Bravo et al., 2023a, 2023b). This new approach highlights the size of cold convective systems and cold cloud cores during heavy rainfall events for austral summer DJF. Furthermore, comparing cold cloud area composites reveals an interesting tendency; cold cloud area and cold cloud cores increase during heavy rainfall events. This is consistent with what has been found in previous geostationary-based studies (Feng et al., 2018, 2021; Lopez-Bravo et al., 2023a; Schumacher & Rasmussen, 2020).

Rainfall related to mesoscale convective systems is one of the main contributors to seasonal rainfall and the hydrological cycle at local and regional scales (Da Silva & Matthews, 2021; Schumacher & Rasmussen, 2020). Our findings on diurnally driven convection and severe weather regimes suggest that heavy rainfall produces sustained precipitation over the mountain ranges and lowlands of Sumatra. This result ties well with recent previous studies wherein the role of heavy and extreme rainfall contribution and diverse effects of mesoscale convective systems have been explored worldwide (Feng et al., 2021; Schumacher & Rasmussen, 2020). These studies have demonstrated the link between heavy rainfall and flash floods and have also shown the effects of extreme rainfall on the population in North America, South America, and East Asia. However, the fraction of total rainfall shows the important contribution of MCS in Feng et al. (2021) and Schumacher and Rasmussen (2020). In addition, our study has provided new insight into cloud variability during the enhanced and suppressed convective phases of the MJO. We have further noted that the intraseasonal sources of variability of heavy rainfall are diverse; rainfall over Sumatra is very sensitive to the amount of water vapor due to large-scale and mesoscale conditions, which are responsible for the transport of water vapor towards regions of the genesis of the diurnally driven convection. These results can be relevant to other modes of variability over Sumatra, including Kelvin waves and ENSO.

5. Conclusions

The aim of the present study was to examine the large-scale and local influence on the fraction of cold cloud tops and rainfall associated with heavy rainfall events over Sumatra during austral summer December-January-February (DJF). This work has used state-of-the-art geostationary observations from Himawari-8 AHI and satellite-based rainfall from IMERG to better understand the occurrence of widespread heavy rainfall over Sumatra and MJO-induced variability and cloud variability linked to heavy rainfall events over Sumatra, which is important for weather and climate prediction. Two analyses were performed to describe the spatial distribution of heavy rainfall in Sumatra and key cloud top characteristics of mesoscale convective systems: (a) satellite-based rainfall from IMERG for DJF (2001–2021) and (b) cold cloud tops from Himawari-8 AHI for DJF (2016–2021). Our results highlight the ability to show high-resolution satellite-based cloud top and rainfall patterns that allows the analysis of the influence of intraseasonal-scale variability over the diurnally driven convection in Sumatra.

We tested the extent to which widespread local and large-scale changes in background winds, moisture, and cloudiness can modulate heavy rainfall and diurnally driven convection over land in Sumatra. However, the relationship is complex because island-scale heavy rainfall differs from localized convection driven by sea breezes and topography forcings. This localized convection can still occur during phases when the MJO is suppressed and is not exclusive to any particular MJO phase. Nevertheless, we find commonalities between all heavy rain events, regardless of the MJO phase, and some changes in the nature of the cloud environment with the MJO phase. The following conclusions can be drawn from the present study:

- The new understanding of heavy rainfall over land based on satellite-rainfall and Precipitation Severity Index has shown that the highest fraction of rainfall on island-scale heavy rainfall days occurs over the central region of Sumatra with a relevant area of influence near Singapore and the Malay Peninsula.
- The study has shown the relevant role of intraseasonal-scale variability of the MJO in modulating the frequency and intensity of heavy rainfall events in Sumatra. MJO phases 2, 3, and 4 exhibit the highest contribution to total daily rainfall with phase 2 showing the strongest rainfall intensity over the land in

Sumatra. However, MJO phase 3 has a notable occurrence of less rainfall intensity events during DJF, which has not been discussed and reported from previous investigations on heavy rainfall and the diurnal cycle of rainfall in the MC (Da Silva & Matthews, 2021; Peatman et al., 2014; Vincent & Lane, 2017).

- There is significant variation with the MJO phase between the cold core area and cold cloud area during heavy rainfall days. We hypothesize that this reflects the proportion of rainfall associated with individual convective towers and MCSs, which reflect the different regimes between MJO suppressed and active phases.

This study has also explored the diurnal signatures of accumulated rainfall over land in Sumatra. The clustering analysis identified six diurnal cycle signatures during the heavy rainfall events over land in Sumatra. Four main diurnal patterns with three subvariants associated with the rainfall intensity over Sumatra were found: (a) these widespread heavy rain events, even though they require large-scale forcing, still have a very pronounced diurnal effect. (b) In the most common clusters (2 and 4), there is also early morning/nighttime rainfall, indicating nondiurnal effects and a large-scale convective environment from the previous day.

One of the findings emerging from this study is that the MJO phase influences the island-scale heavy rainfall while still requiring a significant diurnal component. The MJO-suppressed convective phases (Phases: 7-8-1) showed more local signatures of intense rainfall of the diurnally forced organized convective systems over mountain ranges and the interior area of Sumatra. In phases 2, 3, and 4, the large-scale enhanced convective envelope of the MJO moves over the western MC, and the contribution of heavy rainfall increases over land in Sumatra. Background wind-induced and solar insolation variations reduce during the enhanced convective phases of the MJO over Sumatra. This results in a compound effect of the diurnally driven inland flow associated with the land-sea-breeze system, orographic lifting, and large-scale circulations. As indicated by the moisture flux convergence analysis from ERA5, the amount of moisture transported into the western region of the MC is controlled by the large-scale convective environment-equatorial wave dynamics and its effects over the low-level wind regimes and cyclonic conditions. The effects of large-scale and mesoscale convective environments explain the contribution of heavy rainfall inland Sumatra by MJO phase and other sources of intraseasonal tropical variability.

The influence of large-scale environment and local effects were further examined using the cold cloud top derived from Himawari-8 AHI for six austral summers (DJF, 2016–2021). First, analysis of the brightness temperature from channel 13 (10.4 μm spectral band from Himawari-8 AHI) revealed complex developments of cold cloud populations by MJO phase due to local and nonlocal features over the western region of the MC and the eastern Indian Ocean. Second, the study has also shown that the size and spread of the cold cloud top of convective systems and cold cloud cores increase with the MJO phase during heavy rainfall events relative to all days. Diurnally driven convection in Sumatra is commonly explained as quasilinear convective systems (Lopez-Bravo et al., 2023a; Love et al., 2011; Short et al., 2019; Vincent & Lane, 2016). However, the cold cloud area exceeds 100,000 km^2 with deep cloud tops, and low cloud top temperature, during heavy rainfall events, which supports organized convection and may develop as mesoscale convective complexes, causing severe weather conditions and hazardous rainfall associated with flash flood events in Sumatra.

In general, this study strengthens the understanding of heavy rainfall and cloud population and the effects of the intraseasonal-scale tropical variability over the diurnally driven convection over Sumatra. The findings of this research provide

- insights for describing the local effects and contribution of heavy rainfall to seasonal rainfall inland Sumatra,
- enhancing the comprehension of diurnal rainfall signatures of heavy rainfall events,
- quantifying the influence of large-scale and mesoscale convective environment by MJO phase,
- describing the effects between heavy rainfall events and diurnal evolution of mesoscale convective systems.

Widespread heavy rainfall, as diagnosed by the PSI, is different from localized heavy rainfall and may have critical hydrological implications. The methodology and analysis presented in this paper lay the groundwork for potential prediction or now-casting of such events. Moreover, the finely balanced co-contribution of the local and large-scale forcing highlights the challenge of making climate-scale projections of heavy rainfall in the MC.

21698996, 2025, 19, Downloaded from https://agupubs.onlinelibrary.wiley.com/doi/10.1029/2025JD043493 by National Health And Medical Research Council, Wiley Online Library on [27/11/2025]. See the Terms and Conditions (https://onlinelibrary.wiley.com/terms-and-conditions) on Wiley Online Library for rules of use; OA articles are governed by the applicable Creative Commons License

21698996, 2025, 19, Downloaded from https://agupubs.onlinelibrary.wiley.com/doi/10.1029/2025JD043493 by National Health And Medical Research Council, Wiley Online Library on [27/11/2025]. See the Terms and Conditions (https://onlinelibrary.wiley.com/terms-and-conditions) on Wiley Online Library for rules of use; OA articles are governed by the applicable Creative Commons License

Appendix A: Precipitation Severity Index

The Precipitation Severity Index (PSI) includes rainfall intensity of each grid point, time persistence, and affected area in Equation A1:

$$PSI_T = \frac{1}{(1+d)\cdot A}\sum_{i=1}^{N}\sum_{j=1}^{M}\sum_{t=T-d}^{T}\frac{RR_{i,j,t}}{RR_{\mathrm{perc}_{i,j}}}\cdot(\Delta x)^2\cdot\prod_{\tau=t}^{T} I(RR_{i,j,\tau}, RR_{\mathrm{perc}_{i,j}}) \quad \text{(A1)}$$

$$I(RR_{i,j,\tau}, RR_{\mathrm{perc}_{i,j}}) = \begin{cases} 0 \text{ if } RR_{i,j,\tau} \le RR_{80_{i,j}} \\ 1 \text{ if } RR_{i,j,\tau} > RR_{80_{i,j}} \end{cases}$$

The PSI is calculated as the ratio between the daily accumulated rainfall ($RR_{i,j,t}$) and a percentile of the climatology ($RR_{\mathrm{perc}_{i,j}}$) at each grid point (i, j), and time step $T(PSI_T)$. Different thresholds were tested (80th, 90th, and 95th percentiles) to detect regions with heavy daily rainfall. In this study, we set the threshold as the all-day 80th percentile for each grid point to exclude grid points with precipitation below this value on day $T(RR_{i,j,\tau} \le RR_{\mathrm{perc}_{i,j}})$ by means of the function $I(RR_{i,j,\tau}, RR_{\mathrm{perc}_{i,j}})$. The ratios at each grid point for day T and the previous d days consider a persistence of 2 days considering rainfall was continuous and larger than $RR_{\mathrm{perc}_{i,j}}$ at the same grid points (i,j). The cell size was considered by the area of one grid cell $(\Delta x)^2$. The ratios are summed over the valid grid point over Sumatra $(N \times M)$ along directions i and j. The daily PSI value is normalized by the area of Sumatra $A = N \cdot M \cdot (\Delta x)^2$ and $(1 + d)$ to consider adding grid points with persistent rainfall. Note that A correction for latitude stretching of the grid was performed before the computation of the PSI.

Conflict of Interest

The authors declare no conflicts of interest relevant to this study.

Data Availability Statement

The Himawari-8 GeoCat 1.0.3 Australian Domain Collections Level 1 (Lopez-Bravo et al., 2021a) and Level 2 (Lopez-Bravo et al., 2021b) data sets were used to explore diurnally forced convection over Sumatra. These data sets are available from the NCI National Research Data Collection, Australia, under the Creative Commons Attribution 4.0 International license.

Version 1.1 of the CSPP-Geo GEOCAT package is used to generate cloud property products from Himawari-8 AHI. This software was provided by the Community Satellite Processing Package for Geostationary Data (CSPP Geo) and Cooperative Institute for Meteorological Satellite Studies (CIMSS) (CSPP Geo, CIMSS, 2021).

Acknowledgments
This work was funded by the ARC Centre of Excellence for Climate Extremes CE170100023 for C. Lopez-Bravo, C. Vincent, Y. Huang, and T. P. Lane and the Melbourne Research Scholarship and the Australian Research Council's (ARC) Discovery Project DP190100786 for C. Lopez-Bravo. The production of derived-satellite data from Himawari-8 AHI for this research was undertaken on the NCI National Facility in Canberra, Australia, supported by the Australian Commonwealth Government. The authors sincerely appreciate the three reviewers for their valuable and constructive feedback, which significantly contributed to the improvement of this manuscript. The authors also wish to thank the Meteorological Satellite Center, The Bureau of Meteorology, Australia, and the CSPP Geo project, CIMSS. Open access publishing facilitated by The University of Melbourne, as part of the Wiley - The University of Melbourne agreement via the Council of Australian University Librarians.

References

Bai, H., Deranadyan, G., Schumacher, C., Funk, A., Epifanio, C., Ali, A., et al. (2021). Formation of nocturnal offshore rainfall near the west coast of Sumatra: Land breeze or gravity wave? *Monthly Weather Review*, *149*(3), 715–731. https://doi.org/10.1175/MWR-D-20-0179.1

Baranowski, D. B., Flatau, M. K., Flatau, P. J., Karnawati, D., Barabasz, K., Labuz, M., et al. (2020). Social-media and newspaper reports reveal large-scale meteorological drivers of floods on Sumatra. *Nature Communications*, *11*(1), 1–10. https://doi.org/10.1038/s41467-020-16171-2

Baranowski, D. B., Flatau, M. K., Flatau, P. J., & Matthews, A. J. (2016). Phase locking between atmospheric convectively coupled equatorial Kelvin waves and the diurnal cycle of precipitation over the Maritime Continent. *Geophysical Research Letters*, *43*(15), 8269–8276. https://doi.org/10.1002/2016GL069602

Beucher, S. (1979). Use of watersheds in contour detection. In *Proceedings of the International Workshop on Image Processing*.

Birch, C. E., Webster, S., Peatman, S. C., Parker, D. J., Matthews, A. J., Li, Y., & Hassim, M. E. E. (2016). Scale interactions between the MJO and the Western Maritime Continent. *Journal of Climate*, *29*(7), 2471–2492. https://doi.org/10.1175/JCLI-D-15-0557.1

Caldas-Alvarez, A., Feldmann, H., Lucio-Eceiza, E., & Pinto, J. G. (2022). Scale-dependency of extreme precipitation processes in regional climate simulations of the greater Alpine region. *Weather and Climate Dynamics Discussions*, *2022*, 1–37. https://doi.org/10.5194/wcd-2022-11

Chan, M. Y., Lo, J. C.-F., & Orton, T. (2019). The structure of tropical Sumatra squalls. *Weather*, *74*(5), 176–181. https://doi.org/10.1002/wea.3375

Cheng, Y.-M., Dias, J., Kiladis, G., Feng, Z., & Leung, L. R. (2023). Mesoscale convective systems modulated by convectively coupled equatorial waves. *Geophysical Research Letters*, *50*(10), e2023GL103335. https://doi.org/10.1029/2023GL103335

Crook, J., Morris, F., Fitzpatrick, R. G. J., Peatman, S. C., Schwendike, J., Stein, T. H., et al. (2024). Impact of the Madden–Julian Oscillation and equatorial waves on tracked mesoscale convective systems over Southeast Asia. *Quarterly Journal of the Royal Meteorological Society*, *150*(760), 1724–1751. https://doi.org/10.1002/qj.4667

CSPP Geo, CIMSS. (2021). CSPP Geo GEOCAT package (Version 1.1) [Software]. Retrieved January 2021, from http://cimss.ssec.wisc.edu/csppgeo/geocat.html

Da Silva, N. A., & Matthews, A. J. (2021). Impact of the Madden–Julian Oscillation on extreme precipitation over the western Maritime Continent and Southeast Asia. *Quarterly Journal of the Royal Meteorological Society*, *147*(739), 3434–3453. https://doi.org/10.1002/qj.4136

Da Silva, N. A., Webber, B. G. M., Matthews, A. J., Feist, M. M., Stein, T. H. M., Holloway, C. E., & Abdullah, M. F. A. B. (2021). Validation of GPM IMERG extreme precipitation in the maritime continent by station and radar data. *Earth and Space Science*, *8*(7), e2021EA001738. https://doi.org/10.1029/2021EA001738

Dias, J., Sakaeda, N., Kiladis, G. N., & Kikuchi, K. (2017). Influences of the MJO on the space-time organization of tropical convection. *Journal of Geophysical Research: Atmospheres*, *122*(15), 8012–8032. https://doi.org/10.1002/2017JD026526

Feng, Z., Leung, L. R., Houze, R. A., Jr., Hagos, S., Hardin, J., Yang, Q., et al. (2018). Structure and evolution of mesoscale convective systems: Sensitivity to cloud microphysics in convection-permitting simulations over the United States. *Journal of Advances in Modeling Earth Systems*, *10*(7), 1470–1494. https://doi.org/10.1029/2018MS001305

Feng, Z., Leung, L. R., Liu, N., Wang, J., Houze Jr, R. A., Li, J., et al. (2021). A global high-resolution mesoscale convective system database using satellite-derived cloud tops, surface precipitation, and tracking. *Journal of Geophysical Research: Atmospheres*, *126*(8), e2020JD034202. https://doi.org/10.1029/2020JD034202

Ferrett, S., Yang, G.-Y., Woolnough, S. J., Methven, J., Hodges, K., & Holloway, C. E. (2020). Linking extreme precipitation in Southeast Asia to equatorial waves. *Quarterly Journal of the Royal Meteorological Society*, *146*(727), 665–684. https://doi.org/10.1002/qj.3699

Fiddes, S., Pepler, A., Saunders, K., & Hope, P. (2021). Redefining southern Australia's climatic regions and seasons. *Journal of Southern Hemisphere Earth Systems Science*, *71*(1), 92–109. https://doi.org/10.1071/es20003

Fine, C. M., Johnson, R. H., Ciesielski, P. E., & Taft, R. K. (2016). The role of topographically induced vortices in tropical cyclone formation over the Indian Ocean. *Monthly Weather Review*, *144*(12), 4827–4847. https://doi.org/10.1175/MWR-D-16-0102.1

Fiolleau, T., & Roca, R. (2013). An algorithm for the detection and tracking of tropical mesoscale convective systems using infrared images from geostationary satellite. *IEEE Transactions on Geoscience and Remote Sensing*, *51*(7), 4302–4315. https://doi.org/10.1109/TGRS.2012.2227762

Hardy, S., Methven, J., Schwendike, J., Harvey, B., & Cullen, M. (2023). Examining the dynamics of a Borneo vortex using a balance approximation tool. *Weather and Climate Dynamics*, *4*(4), 1019–1043. https://doi.org/10.5194/wcd-4-1019-2023

Hastie, T., Tibshirani, R., & Friedman, J. (2009). The elements of statistical learning: Data mining, inference, and prediction. In *Springer series in statistics*. Springer. New York.

Heikenfeld, M., Marinescu, P., Christensen, M., Watson-Parris, D., Senf, F., Heever, S., & Stier, P. (2019). tobac v1.0: Towards a flexible framework for tracking and analysis of clouds in diverse datasets. *Geoscientific Model Development Discussions*, 1–31. https://doi.org/10.5194/gmd-2019-105

Hersbach, H., Bell, B., Berrisford, P., Hirahara, S., Horányi, A., Muñoz-Sabater, J., et al. (2020). The ERA5 global reanalysis. *Quarterly Journal of the Royal Meteorological Society*, *146*(730), 1999–2049. https://doi.org/10.1002/qj.3803

Huffman, G., Bolvin, D., Braithwaite, D., Hsu, K., Joyce, R., Kidd, C., et al. (2019). NASA global precipitation measurement (GPM) integrated multi-satellite retrievals for GPM (IMERG). In *Algorithm theoretical basis document (ATBD) Version 06*. National Aeronautics and Space Administration (NASA).

Huffman, G., Stocker, E., Bolvin, D., Nelkin, E., & Tan, J. (2019). *GPM IMERG final precipitation L3 half hourly 0.1 degree x 0.1 degree V06*. Goddard Earth Sciences Data and Information Services Center (GES DISC), National Aeronautics and Space Administration (NASA). Greenbelt, MD.

Huffman, G. J., Bolvin, D. T., Braithwaite, D., Hsu, K.-L., Joyce, R. J., Kidd, C., et al. (2020). Integrated multi-satellite retrievals for the global precipitation measurement (GPM) mission (IMERG). *Advances in Global Change Research*, 343–353. https://doi.org/10.1007/978-3-030-24568-9_19

JMA. (2017). *Himawari–8/9 Himawari standard data user's guide (Version 1.3)*. Japan Meteorological Agency Tokyo, Japan.

Johnson, P., Ciesielski, P., Fine, C., & Wang, C. (2023). Effects of the topography of Sumatra on tropical cyclone formation over the Indian Ocean. *MAUSAM: Quarterly Journal of Meteorology, Hydrology & Geophysics*, *74*(2), 389–396. https://doi.org/10.54302/mausam.v74i2.6062

Kerns, B. W., & Chen, S. S. (2018). Diurnal cycle of precipitation and cloud clusters in the MJO and ITCZ over the Indian Ocean. *Journal of Geophysical Research: Atmospheres*, *123*(18), 10140–10161. https://doi.org/10.1029/2018JD028589

Kiladis, G. N., Wheeler, M. C., Haertel, P. T., Straub, K. H., & Roundy, P. E. (2009). Convectively coupled equatorial waves. *Reviews of Geophysics*, *47*(2). https://doi.org/10.1029/2008RG000266

Koseki, S., Koh, T.-Y., & Teo, C.-K. (2014). Borneo vortex and mesoscale convective rainfall. *Atmospheric Chemistry and Physics*, *14*(9), 4539–4562. https://doi.org/10.5194/acp-14-4539-2014

Latos, B., Lefort, T., Flatau, M. K., Flatau, P. J., Permana, D. S., Baranowski, D. B., et al. (2021). Equatorial waves triggering extreme rainfall and floods in Southwest Sulawesi, Indonesia. *Monthly Weather Review*, *149*(5), 1381–1401. https://doi.org/10.1175/MWR-D-20-0262.1

Leckebusch, G. C., Renggli, D., & Ulbrich, U. (2008). Development and application of an objective storm severity measure for the Northeast Atlantic region. *Meteorologische Zeitschrift*, *17*(5), 575–587. https://doi.org/10.1127/0941-2948/2008/0323

Lopez-Bravo, C., Vincent, C. L., & Huang, Y. (2021a). Himawari-8 GeoCat 1.0.3 Australian Domain Level 1 v1.0 [Dataset]. *NCI National Research Data Collection*. https://doi.org/10.25914/60096221a8f7a

Lopez-Bravo, C., Vincent, C. L., & Huang, Y. (2021b). Himawari-8 GeoCat 1.0.3 Australian Domain Level 2 v1.0 [Dataset]. *NCI National Research Data Collection*. https://doi.org/10.25914/60096228c7ec0

Lopez-Bravo, C., Vincent, C. L., Huang, Y., & Lane, T. P. (2023a). A case study of a west Sumatra squall line using satellite observations. *Monthly Weather Review*, *151*(2), 523–543. https://doi.org/10.1175/MWR-D-21-0194.1

Lopez-Bravo, C., Vincent, C. L., Huang, Y., & Lane, T. P. (2023b). The diurnal cycle of rainfall and deep convective clouds around Sumatra and the associated MJO-induced variability during austral summer in Himawari-8. *Journal of Geophysical Research: Atmospheres*, *128*(22), e2023JD039132. https://doi.org/10.1029/2023JD039132

Love, B. S., Matthews, A. J., & Lister, G. M. S. (2011). The diurnal cycle of precipitation over the Maritime Continent in a high-resolution atmospheric model. *Quarterly Journal of the Royal Meteorological Society*, *137*(657), 934–947. https://doi.org/10.1002/qj.809

Machado, L. A. T., Duvel, J.-P., & Desbois, M. (1993). Diurnal variations and modulation by easterly waves of the size distribution of convective cloud clusters over West Africa and the Atlantic Ocean. *Monthly Weather Review*, *121*(1), 37–49. https://doi.org/10.1175/1520-0493(1993)121⟨0037:DVAMBE⟩2.0.CO;2

Madden, R. A., & Julian, P. R. (1971). Detection of a 40–50 day oscillation in the zonal wind in the Tropical Pacific. *Journal of the Atmospheric Sciences*, *28*(5), 702–708. https://doi.org/10.1175/1520-0469(1971)028⟨0702:DOADOI⟩2.0.CO;2

Maloney, E. D., & Hartmann, D. L. (1998). Frictional moisture convergence in a composite life cycle of the Madden–Julian Oscillation. *Journal of Climate*, *11*(9), 2387–2403. https://doi.org/10.1175/1520-0442(1998)011⟨2387:FMCIAC⟩2.0.CO;2

21698996, 2025, 19, Downloaded from https://agupubs.onlinelibrary.wiley.com/doi/10.1029/2025JD043493 by National Health And Medical Research Council, Wiley Online Library on [27/11/2025]. See the Terms and Conditions (https://onlinelibrary.wiley.com/terms-and-conditions) on Wiley Online Library for rules of use; OA articles are governed by the applicable Creative Commons License

Mapes, B., Tulich, S., Lin, J., & Zuidema, P. (2006). The mesoscale convection life cycle: Building block or prototype for large-scale tropical waves? *Dynamics of Atmospheres and Oceans*, *42*(1), 3–29. https://doi.org/10.1016/j.dynatmoce.2006.03.003

Mapes, B. E., & Houze, R. A. (1993). Cloud clusters and superclusters over the oceanic warm pool. *Monthly Weather Review*, *121*(5), 1398–1416. https://doi.org/10.1175/1520-0493(1993)121⟨1398:CCASOT⟩2.0.CO;2

Matthews, A. J. (2000). Propagation mechanisms for the Madden-Julian Oscillation. *Quarterly Journal of the Royal Meteorological Society*, *126*(569), 2637–2651. https://doi.org/10.1002/qj.49712656902

Mori, S., Jun-Ichi, H., Tauhid, Y. I., Yamanaka, M. D., Okamoto, N., Murata, F., et al. (2004). Diurnal land-sea rainfall peak migration over Sumatera Island, Indonesian Maritime Continent, observed by TRMM satellite and intensive Rawinsonde soundings. *Monthly Weather Review*, *132*(8), 2021–2039. https://doi.org/10.1175/1520-0493(2004)132⟨2021:DLRPMO⟩2.0.CO;2

Nakazawa, T. (1988). Tropical super clusters within intraseasonal variations over the Western Pacific. *Journal of the Meteorological Society of Japan*, *66*(6), 823–839. https://doi.org/10.2151/jmsj1965.66.6_823

Natoli, M. B., & Maloney, E. D. (2023a). Environmental controls on the tropical island diurnal cycle in the context of intraseasonal variability. *Journal of Climate*, *36*(21), 7465–7485. https://doi.org/10.1175/JCLI-D-22-0824.1

Natoli, M. B., & Maloney, E. D. (2023b). The tropical diurnal cycle under varying states of the monsoonal background wind. *Journal of the Atmospheric Sciences*, *80*(1), 235–258. https://doi.org/10.1175/JAS-D-22-0045.1

Nesbitt, S. W., Cifelli, R., & Rutledge, S. A. (2006). Storm morphology and rainfall characteristics of TRMM precipitation features. *Monthly Weather Review*, *134*(10), 2702–2721. https://doi.org/10.1175/MWR3200.1

Oh, J.-H., Kim, K.-Y., & Lim, G.-H. (2012). Impact of MJO on the diurnal cycle of rainfall over the western Maritime Continent in the austral summer. *Climate Dynamics*, *38*(5), 1167–1180. https://doi.org/10.1007/s00382-011-1237-4

Peatman, S. C., Birch, C. E., Schwendike, J., Marsham, J. H., Dearden, C., Webster, S., et al. (2023). The role of density currents and gravity waves in the offshore propagation of convection over Sumatra. *Monthly Weather Review*, *151*(7), 1757–1777. https://doi.org/10.1175/MWR-D-22-0322.1

Peatman, S. C., Matthews, A. J., & Stevens, D. P. (2014). Propagation of the Madden–Julian Oscillation through the Maritime Continent and scale interaction with the diurnal cycle of precipitation. *Quarterly Journal of the Royal Meteorological Society*, *140*(680), 814–825. https://doi.org/10.1002/qj.2161

Peatman, S. C., Schwendike, J., Birch, C. E., Marsham, J. H., Matthews, A. J., & Yang, G.-Y. (2021). A local-to-large scale view of maritime continent rainfall: Control by ENSO, MJO, and equatorial waves. *Journal of Climate*, *34*(22), 8933–8953. https://doi.org/10.1175/JCLI-D-21-0263.1

Pinto, J. G., Karremann, M. K., Born, K., Della-Marta, P. M., & Klawa, M. (2012). Loss potentials associated with European windstorms under future climate conditions. *Climate Research*, *54*(1), 1–20. https://doi.org/10.3354/cr01111

Piper, D., Kunz, M., Ehmele, F., Mohr, S., Mühr, B., Kron, A., & Daniell, J. (2016). Exceptional sequence of severe thunderstorms and related flash floods in May and June 2016 in Germany—Part 1: Meteorological background. *Natural Hazards and Earth System Sciences*, *16*(12), 2835–2850. https://doi.org/10.5194/nhess-16-2835-2016

Qian, J.-H. (2008). Why precipitation is mostly concentrated over islands in the maritime continent. *Journal of the Atmospheric Sciences*, *65*(4), 1428–1441. https://doi.org/10.1175/2007JAS2422.1

Ramadhan, R., Marzuki, M., Yusnaini, H., Muharsyah, R., Suryanto, W., Sholihun, S., et al. (2022). Capability of GPM IMERG products for extreme precipitation analysis over the Indonesian Maritime Continent. *Remote Sensing*, *14*(2), 412. https://doi.org/10.3390/rs14020412

Rauniyar, S. P., & Walsh, K. J. E. (2011). Scale interaction of the diurnal cycle of rainfall over the Maritime Continent and Australia: Influence of the MJO. *Journal of Climate*, *24*(2), 325–348. https://doi.org/10.1175/2010JCLI3673.1

Roca, R., & Fiolleau, T. (2020). Extreme precipitation in the tropics is closely associated with long-lived convective systems. *Communications Earth & Environment*, *1*(1), 1–6. https://doi.org/10.1038/s43247-020-00015-4

Ruppert, J. H., & Chen, X. (2020). Island rainfall enhancement in the maritime continent. *Geophysical Research Letters*, *47*(5), e2019GL086545. https://doi.org/10.1029/2019GL086545

Sakaeda, N., Kiladis, G., & Dias, J. (2020). The diurnal cycle of rainfall and the convectively coupled equatorial waves over the maritime continent. *Journal of Climate*, *33*(8), 3307–3331. https://doi.org/10.1175/JCLI-D-19-0043.1

Sakurai, N., Murata, F., Yamanaka, M. D., Mori, S., Hamada, J.-I., Hashiguchi, H., et al. (2005). Diurnal cycle of cloud system migration over Sumatera Island. *Journal of the Meteorological Society of Japan*, *83*(5), 835–850. https://doi.org/10.2151/jmsj.83.835

Salby, M. L., & Hendon, H. H. (1994). Intraseasonal behavior of clouds, temperature, and motion in the tropics. *Journal of the Atmospheric Sciences*, *51*(15), 2207–2224. https://doi.org/10.1175/1520-0469(1994)051⟨2207:IBOCTA⟩2.0.CO;2

Schumacher, R. S., & Rasmussen, K. L. (2020). The formation, character and changing nature of mesoscale convective systems. *Nature Reviews Earth & Environment*, *1*(6), 300–314. https://doi.org/10.1038/s43017-020-0057-7

Senior, N. V., Matthews, A. J., Webber, B. G. M., Webster, S., Jones, R. W., Permana, D. S., et al. (2023). Extreme precipitation at Padang, Sumatra triggered by convectively coupled kelvin waves. *Quarterly Journal of the Royal Meteorological Society*, *149*(755), 2281–2300. https://doi.org/10.1002/qj.4506

Short, E., Vincent, C. L., & Lane, T. P. (2019). Diurnal cycle of surface winds in the maritime continent observed through satellite scatterometry. *Monthly Weather Review*, *147*(6), 2023–2044. https://doi.org/10.1175/MWR-D-18-0433.1

Tan, J., Huffman, G. J., Bolvin, D. T., & Nelkin, E. J. (2019). Diurnal cycle of IMERG V06 precipitation. *Geophysical Research Letters*, *46*(22), 13584–13592. https://doi.org/10.1029/2019GL085395

Tapiador, F. J., Navarro, A., García-Ortega, E., Merino, A., Sánchez, J. L., Marcos, C., & Kummerow, C. (2020). The contribution of rain gauges in the calibration of the IMERG product: Results from the first validation over Spain. *Journal of Hydrometeorology*, *21*(2), 161–182. https://doi.org/10.1175/JHM-D-19-0116.1

Vila, D. A., Machado, L. A. T., Laurent, H., & Velasco, I. (2008). Forecast and tracking the evolution of cloud clusters (ForTraCC) using satellite infrared imagery: Methodology and validation. *Weather and Forecasting*, *23*(2), 233–245. https://doi.org/10.1175/2007WAF2006121.1

Vincent, C. L., & Huang, Y. (2022). Meso- and microscale response to variation in cloudiness at three forested sites in the Maritime Continent. *Quarterly Journal of the Royal Meteorological Society*, *148*(742), 418–433. https://doi.org/10.1002/qj.4212

Vincent, C. L., & Lane, T. P. (2016). Evolution of the diurnal precipitation cycle with the passage of a Madden-Julian Oscillation event through the maritime continent. *Monthly Weather Review*, *144*(5), 1983–2005. https://doi.org/10.1175/MWR-D-15-0326.1

Vincent, C. L., & Lane, T. P. (2017). A 10-Year Austral summer climatology of observed and modeled intraseasonal, mesoscale, and diurnal variations over the maritime continent. *Journal of Climate*, *30*(10), 3807–3828. https://doi.org/10.1175/JCLI-D-16-0688.1

Watters, D., Battaglia, A., & Allan, R. P. (2021). The diurnal cycle of precipitation according to multiple decades of global satellite observations, Three CMIP6 models, and the ECMWF reanalysis. *Journal of Climate*, *34*(12), 5063–5080. https://doi.org/10.1175/JCLI-D-20-0966.1

21698996, 2025, 19, Downloaded from https://agupubs.onlinelibrary.wiley.com/doi/10.1029/2025JD043493 by National Health And Medical Research Council, Wiley Online Library on [27/11/2025]. See the Terms and Conditions (https://onlinelibrary.wiley.com/terms-and-conditions) on Wiley Online Library for rules of use; OA articles are governed by the applicable Creative Commons License

Wei, Y., Pu, Z., & Zhang, C. (2020). Diurnal cycle of precipitation over the maritime continent under modulation of MJO: Perspectives from cloud-permitting scale simulations. *Journal of Geophysical Research: Atmospheres*, *125*(13), e2020JD032529. https://doi.org/10.1029/2020JD032529

Wheeler, M., & Hendon, H. H. (2004). An all-season real-time multivariate MJO Index: Development of an index for monitoring and prediction. *Monthly Weather Review*, *132*(8), 1917–1932. https://doi.org/10.1175/1520-0493(2004)132⟨1917:AARMMI⟩2.0.CO;2

Wu, P., Mori, S., Hamada, J.-I., Yamanaka, M. D., Matsumoto, J., & Kimura, F. (2008). Diurnal variation of rainfall and precipitable water over Siberut Island off the Western Coast of Sumatra Island. *SOLA*, *4*, 125–128. https://doi.org/10.2151/sola.2008-032

Xavier, P., Rahmat, R., Cheong, W. K., & Wallace, E. (2014). Influence of Madden-Julian Oscillation on Southeast Asia rainfall extremes: Observations and predictability. *Geophysical Research Letters*, *41*(12), 4406–4412. https://doi.org/10.1002/2014GL060241

Yokoi, S., Mori, S., Katsumata, M., Geng, B., Yasunaga, K., Syamsudin, F., et al. (2017). Diurnal cycle of precipitation observed in the western coastal area of Sumatra Island: Offshore preconditioning by gravity waves. *Monthly Weather Review*, *145*(9), 3745–3761. https://doi.org/10.1175/MWR-D-16-0468.1

You, Y., Meng, H., Dong, J., & Rudlosky, S. (2019). Time-lag correlation between passive microwave measurements and surface precipitation and its impact on precipitation retrieval evaluation. *Geophysical Research Letters*, *46*(14), 8415–8423. https://doi.org/10.1029/2019GL083426

Zipser, E. J., Cecil, D. J., Liu, C., Nesbitt, S. W., & Yorty, D. P. (2006). Where are the most intense thunderstorms on Earth? *Bulletin of the American Meteorological Society*, *87*(8), 1057–1072. https://doi.org/10.1175/BAMS-87-8-1057

21698996, 2025, 19, Downloaded from https://agupubs.onlinelibrary.wiley.com/doi/10.1029/2025JD043493 by National Health And Medical Research Council, Wiley Online Library on [27/11/2025]. See the Terms and Conditions (https://onlinelibrary.wiley.com/terms-and-conditions) on Wiley Online Library for rules of use; OA articles are governed by the applicable Creative Commons License